Fábio Miguel Ferreira Vieira

Licenciado em Ciências de Engenharia de Micro e Nanotecnologias

Sunlight-driven CO_2 Conversion: Producing Methane with Photovoltaics

Dissertação para obtenção do Grau de Mestre em
Engenharia de Micro e Nanotecnologia

Orientador: Dr. Manuel J. Mendes, Professor Auxiliar Convidado,

Faculdade de Ciências e Tecnologia, Universidade Nova de Lisboa

Co-orientador: Dra. Ana Machado, Investigadora Auxiliar,

Faculdade de Ciências e Tecnologia, Universidade Nova de Lisboa

Júri:

Presidente: Dr. Luís Miguel Nunes Pereira

Arguente: Dr. Carmen Mireya Rangel Archila

Vogais: Dr. Manuel João de Moura Mendes

FACULDADE DE CIÊNCIAS E TECNOLOGIA
UNIVERSIDADE NOVA DE LISBOA

Sunlight-driven CO_2 Conversion: Producing Methane with Photovoltaics

Acknowledgements

Antes de mais, gostaria de agradecer ao Dr. Rodrigo Martins, presidente do departamento de ciência dos materiais (DCM), e à Dra. Elvira Fortunato, diretora do centro de investigação de materiais (CENIMAT), por criarem este curso único, a que me dediquei nestes ultimos anos. Quero também fazer um agradecimento especial ao Dr. Manuel Mendes, meu orientador, e à Dra. Ana Reis Machado, minha co-orientadora, pela oportunidade de trabalhar neste tema inovador e pela ajuda prestada sempre que a solicitei. Um agradecimento também a todos os professores que me acompanharam durante estes 5 anos, que me guiaram até este ponto.

Quero agradecer também a todos os colegas que me acompanharam durante estes 5 anos, com quem travei amizades duradouras por entre trabalho, dedicação e muitas festas e finais de tarde passados com excelente companhia. Um especial agradecimento ao Manuel e ao Miguel, que embarcaram nesta aventura que é a simulação juntamente comigo, ao Bernardo por toda a troca de ideias e entreajuda durante estes ultimos meses e à Debora, ao Lima, à Rita, ao Teles e à Péssima por todo o apoio, amizade e entreajuda durante estes anos.

Gostaria ainda de agradecer ao meu grande grupo de amigos que me acompanham desde o secundário, Rita Caneco, Rita Mateus, Mariana, Coelho, Henrique, Rosa, Gonçalo e Guizadas, por me proporcionarem quase todas as semanas um grande alívio de stress. Que continuemos juntos por muitos e bons anos e arranjemos sempre tempo para um café e um joguinho de setas.

O maior dos meus obrigados à minha família que tanto me apoio durante todos estes anos de estudo, aos meus pais, por todo o que me proporcionaram e que tiveram de aturar durante 23 anos, aos meus irmãos e aos seus esposos, por toda a confiança e apoio prestados e por terem sempre uma porta aberta nas suas casas e, por fim, aos meus sobrinhos Gonçalo, Beatriz, Afonso, Constança e Leonor, a quem dedico este trabalho, pois motivam-me todos os dias a ser a melhor pessoa de modo a transmitir-vos o melhor exemplo possível.

Abstract

Due to greenhouse gas emissions, CO_2 capture and utilization (CCU) technologies are being immensely researched. In these technologies, CO_2 from gas emissions or directly from the atmosphere is converted into chemical products. One of these technologies is artificial photosynthesis, which uses solar energy, carbon dioxide and water to generate hydrocarbon fuels, being methane (CH_4) a preferential target due to the already in place infrastructures for its storage, distribution and consumption. Based on electrochemical kinetic models, two different approaches to the production of CH_4 via artificial photosynthesis were modelled. One approach was a 1-step transformation of CO_2 and water into CH_4 in a solar powered electrochemical cell (EC). The other was a more conventional 2-step production starting with the solar powered synthesis of an intermediate fuel - syngas (a mixture of carbon monoxide (CO) and molecular hydrogen (H_2) - followed by the conversion of syngas to CH_4 via a Fischer-Tropsch process. The results of the developed simulations reveal that the 1-step method could be applied to a domestic, small scale use, potentially providing energy for a single-family house, whilst the 2-step method can be used in small and large scales applications, from domestic to industrial applications. In terms of overall solar-to-CH_4 energy efficiency, the 2-step method reaches a value of 13.63 % against the 9.18 % reached by the 1-step method.

Keywords: Artificial photosynthesis, Photovoltaic-powered Electrochemical conversion, CO_2 electrolysis, Fisher-Tropsch synthesis, Analytical Modelling, Carbon-based fuels as renewable energy vectors

Resumo

Devido às emissões de gases com efeito de estufa, tecnologias de captura e utilização de CO_2 têm sido intensamente investigadas, sendo o CO_2 proveniente de emissões gasosas ou capturado diretamente da atmosfera convertido em produtos químicos. A fotossíntese artificial é uma destas tecnologias, que utiliza energia solar, dióxido de carbono e água para produzir produtos químicos. O metano (CH_4) é um produto preferencial, devido a já se encontrarem implementadas infraestruturas para o seu armazenamento, distribuição e consumo. Utilizando modelos de cinética eletroquímica, foram modeladas duas abordagens diferentes para a produção de CH_4 através da fotossíntese artificial. Uma abordagem foi a conversão direta de CO_2 e água em metano numa célula eletroquímica alimentada por um sistema fotovoltaico. A outra foi uma conversão convencional de duas etapas, a primeira sendo a produção alimentada a energia solar de um combustível percursor - gás de síntese (uma mistura de monóxido de carbono (CO) e hidrogénio molecular (H_2)) - numa célula eletroquímica, seguida da conversão desse percursor em CH_4 por via de uma síntese de Fischer-Tropsch. Os resultados dessas simulações mostram que o primeiro método (1-etapa) é apropriado para um uso a uma escala mais pequena, potencialmente fornecendo energia para uma casa, enquanto o segundo método (2-etapas) pode ser aplicado em usos domésticos ou industriais. Em termos de eficiência energética, o segundo método tem uma eficiência de 13.63 % enquanto que o primeiro método tem uma eficiência energética de 9.18 %.

Palavras-chave: Fotossíntese artificial, Conversão eletroquímica alimentada por fotovoltaicos, Eletrólise de CO_2, Síntese de Fisher-Tropsch, Modelação Analítica Combustíveis baseados em carbono como fontes de energia renovável

Table of Contents

List of Figures

List of Tables

Abbreviations

CCU – Carbon Capture and Utilization

EC - Electrochemical Cell

FTS – Fischer-Tropsch Synthesis

HTFTS – High Temperature Fischer-Tropsch Synthesis

I-V - Current-Voltage

LTFTS – Low Temperature Fischer-Tropsch Synthesis

PV – Photovoltaic

P-V – Power-Voltage

Syngas – Synthesis gas ($CO+H_2$)

Symbols

α_a – Anodic transfer coefficient

α_c – Cathodic transfer coefficient

η – Overpotential [v]

ΔH^0_C – Enthalpy of adsorption for C [J/mol]

ΔH^0_H – Enthalpy of adsorption for H [J/mol]

A – Rate constant [$mol/Kg_{cat}.s$]

A^0 – Activation energy in standard conditions [J/mol]

c_p – specific heat [kJ/kg.K]

E^0 – Equilibrium potential in standard conditions [V]

E.E. – Energy efficiency

e^- - Electron

e_f – Faradaic efficiency

F – Faraday's constant [C/mol]

h – heat flow rate [kW]

I – Current [A]

I_{mpp} – Current for the maximum power point [A]

I_{SC} – Short circuit current [A]

j – Current density [A/cm^2]

j_0 – Exchange-current density [A/cm^2]

$k^0_{1,18\%Ni}$ – Preexponential factor of rate coefficient $k_{1,18\%Ni}$ [$mol/Kg_{cat}.s$]

$k^0_{1,50\%Ni}$ – Preexponential factor of rate coefficient $k_{1,50\%Ni}$ [$mol/Kg_{cat}.s$]

$k_{1,18\%Ni}$ – Rate coefficient of CO for a 18%Ni-based catalyst [$mol/Kg_{cat}.s$]

$k_{1,50\%Ni}$ – Rate coefficient of CO for a 50%Ni-based catalyst [$mol/Kg_{cat}.s$]

k_{Fe} – Adsorption coefficient for Fe

k_{Co} – Adsorption coefficient for Co

K^0_C – Preexponential factor of adsorption constant for carbon

K^0_H – Preexponential factor of adsorption constant for hydrogen

K_C – Adsorption constant for carbon

K_H – Adsorption constant for hydrogen

m_i – Number of moles of species *i* [mol]

n_i – Number of electrons transferred in the formation of species *i*

P – Power [W]

P_{mpp} – Power for the maximum power point [W]

P_{CO} – Partial Pressure of CO [bar]

P_{H2} – Partial Pressure of H_2 [bar]

Q – Charge [A/s]

q – flow rate [m^3/s]

R – Ideal Gas constant [J/mol.K]

T – Temperature [K]

V – Voltage [V]

V_{mpp} – Voltage for the maximum power point [V]

V_{OC} – Open circuit voltage

Motivation and Objectives

The continuous use of fossil fuels is causing rampant emissions of greenhouse gases to the atmosphere, threatening earth's ecosystems by changing the global climate. Whilst clean fuel alternatives such as solar, wind and hydro are being studied, the atmosphere has still serious concentration levels of greenhouse gases. Artificial photosynthesis is a man-made process that is based of the photosynthesis process in nature, consisting in harvesting solar energy and use that energy to produce fuels made from water and carbon dioxide, being the latter one of the most important greenhouse gases. Artificial photosynthesis produces clean fuels while reducing the atmospheric concentration of greenhouse gases, becoming an attractive technology for the future, making extensive research necessary to understand this technology and adapt it to everyday life.

This work aims to comprehend and design viable methods of using artificial photosynthesis to produce hydrocarbon-based fuels, more particularly methane. This technology is still a relatively new concept and, as such, simulation of its performance in different contexts is important as a preemptive study of its behavior.

I. Introduction

Continuous usage of carbon-rich fossil fuels — coal, oil and natural gas — to produce energy has brought forth an unprecedented era of advancements for human society. However, this caused an increasing CO_2 concentration in the atmosphere, changing from 278 ppm, before the industrial revolution, to 403 ppm in 2016 [1], [2]. This higher concentration is a major contributor to the greenhouse effect, causing temperature raises and climatic changes. Therefore, the capture and transformation of carbon dioxide, via artificial photosynthesis, into hydrocarbons, could lead to the beginning of a carbon-neutral society [1]–[10]. The most researched artificial photosynthesis process is the production of molecular hydrogen by splitting water. This process has reached record solar-to-fuel efficiencies over 16 % [11].

Artificial photosynthesis mimics the original process found in nature, utilizing an electrochemical cell (EC) powered by a photovoltaic (PV) system, with a feedstock of CO_2 and water. This process can be used to produce various sustainable hydrocarbon fuels, effectively producing fuel while consuming one of the major greenhouse gases and providing a clean alternative to fossil fuels, with the advantage of room temperature operation [12]–[15]. This capture and transformation of CO_2 through solar power is a closed-loop fuel cycle - effectively producing carbon-neutral fuels. It should be noted, however, that the splitting of CO_2 is a complex process and it presents great technological challenges in achieving high efficiencies. Thus, the development of a trustworthy method to simulate this process is imperative [1], [10], [12]–[18].

In this work, a comprehensive simulation of methane (CH_4) production is studied. Methane is one of the simplest hydrocarbons and infrastructures for its storage, distribution and consumption are already in place [17], [19]. Therefore, methane is considered to be an attractive hydrocarbon to produce. There are two major approaches, shown in Figure I.1, to this production. One is a 1-Step reduction of CO_2 into CH_4 in an EC, whilst the other is a 2-Step approach. The first step in this 2-Step approach is the simultaneous reduction of CO_2 and H_2O into synthesis gas (syngas), a gas comprised of CO and H_2. The second step of this approach consists of using the previously formed syngas as feedstock to a Fischer-Tropsch synthesis (FTS), obtaining CH_4. An evaluation of the merits of both approaches is realized in this work, in order to access the best possible usages of them.

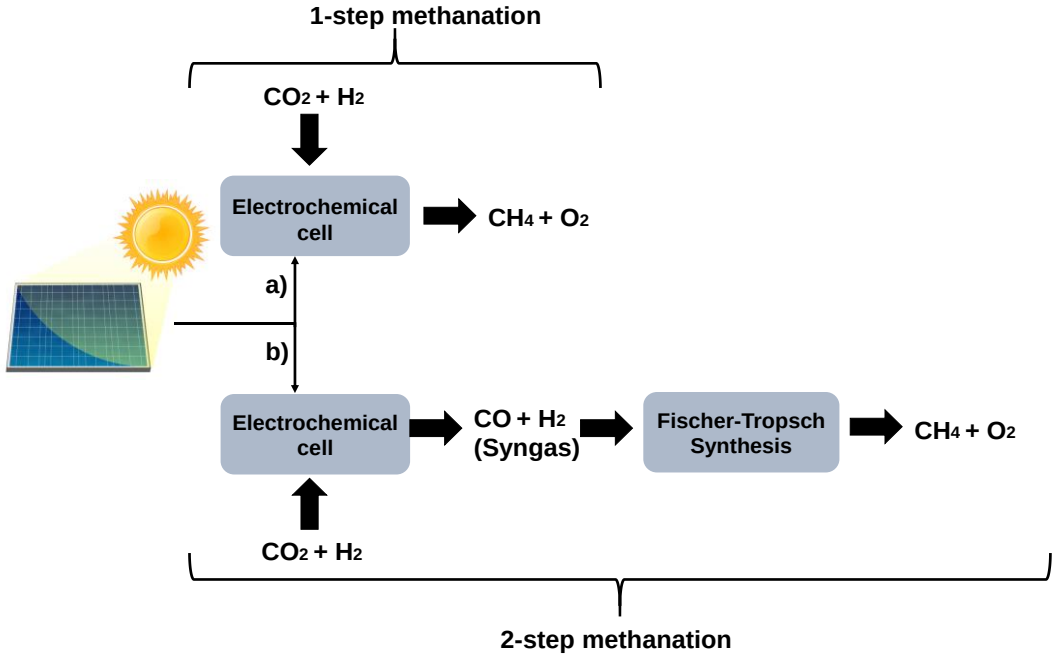

Figure I.1 - The two pathways for methanation studied: a) direct methanation (1-step) pathway, and b) syngas production and FTS methanation (2-step) pathway.

1.1. Water Electrolysis

The most conventional approach for solar fuels production is water splitting via artificial photosynthesis approaches [6], [8], [20], [21]. In this process, water is separated into oxygen and hydrogen via electrochemical reactions promoted by an external stimulus. The stimulus applied could be provided by different energy sources, i.e. light (photolysis), heat (thermolysis) or electricity (electrolysis) [8], [10], [15], [16]. In water electrolysis, a current is driven through two submerged electrodes - the anode and the cathode – with hydrogen being formed on the cathode and oxygen in the anode, but only if enough electric potential is provided to activate the water reduction reactions, since they are occurring are endothermic [1], [21], [22].

At the anode: $$H_2O(l) \rightleftharpoons 2H^+ + \frac{1}{2}O_2 + 2e^- \qquad E^0_{anode} = 1.23\ V \qquad (1)$$

At the cathode: $$2H^+ + 2e^- \rightleftharpoons H_2 \qquad E^0_{cathode} = 0\ V \qquad (2)$$

Global reaction: $$H_2O(l) \rightleftharpoons H_2 + \frac{1}{2}O_2 \qquad E^0_{cell} = 1.23\ V \qquad (3)$$

As seen above, the equilibrium potential (E^0) required to split the water

molecules, at standard conditions, is 1.23 V, although, experimentally, around 1.9 V are required, in order to surpass ohmic losses and electrode defects. This additional potential needed is known as overpotential [6], [15], [18], [21].

1.2. CO_2 Electrolysis

CO_2 electrolysis follows the same principles as water electrolysis. Several products can be formed, depending on how many electron reductions are involved in the reaction [23]. This study will focus in the production of CO, via a 2 electron reduction having H_2 and O_2 as subproducts, allowing the harvest of syngas in the cathode; as well as in the production of CH_4, also called methanation, via a 8 electron reduction having O_2 as a subproduct [10], [17], [23]. The product selectivity mainly depends on the electrocatalyst material used in the cathode, e.g. silver for CO and copper for CH_4, and the provided electric potential.

The main barriers that this technology faces could be improved with better-performing catalysts. Namely, these electrolyzers can only typically operate with high overpotentials, low current densities, and present poor product selectivity - correlating with low faradaic efficiency – leading to a loss of performance over time. Faradaic efficiency describes how efficiently charges are transferred in a electrochemical reaction [10]. Copper is the favorite electrocatalyst for CH_4 synthesis, combining substantial current densities with reasonable overpotentials and faradaic efficiency [1], [2], [10], [16], [17], [23]–[25], and silver is the preferred for syngas production [1]–[3], [10], [15], [16], [24], [26]. For the anode, iridium oxide (IrO_2) is the preferred material [1], [6], [9], [14], [16]–[18], [24], [25], [27]–[33]. Next are presented the global equations for methanation (4) and syngas production (5):

$$\text{Methanation}: \quad CO_2 + 2H_2O \rightleftharpoons CH_4 + 2O_2 \qquad E^0_{cell} = 1.06\ V \tag{4}$$

$$\text{Syngas synthesis}: \quad CO_2 \rightleftharpoons CO + \frac{1}{2}O_2 \qquad E^0_{cell} = 1.34\ V \tag{5}$$

The reduction of CO_2 into CO requires higher activation energy than the methanation. However, the overpotential of the latter is much higher due to the complexity of methanation, associated with 8 electronic reductions, and selectivity issues linked with methane production. Overall, CO_2 reduction into CO has higher efficiency and yield than methanation, being reported energy efficiencies of 60% by Martín, Larrazábal and Pérez-Ramírez (2015) [6], [19], [23], [34]. Nonetheless, with methanation, CH_4 is obtained in a single step process, while for CO reduction, an additional step (2-Step) is required to convert syngas into CH_4.

Another issue that arises with CO_2 electrolysis is the competition between CO_2 reduction and water reduction, making it difficult to single out only one. This occurs due to CO_2 and H_2O equilibrium potentials whose similarity leads to low faradaic efficiencies. In methanation, due to the larger gap between the equilibrium potentials and consequent of the use of Cu, it is possible to achieve more reasonable faradaic efficiencies [19], [35]. In Figure I.2, a schematic of a possible electrochemical cell is shown.

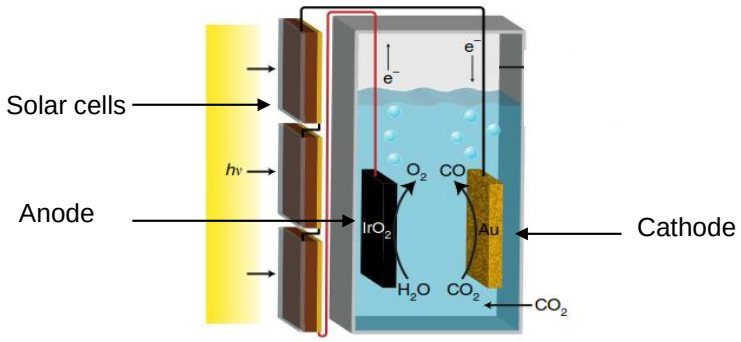

Figure I.2 - Schematic of an electrochemical cell powered up by a photovoltaic (PV) system comprising 3 series connected Perovskite solar cells. The series interconnection is necessary to allow the PV module to supply the required photovoltage to drive the reaction with reasonable yield of synthesized products. This cell is used to produce CO using Au as a cathode. Adapted from [18].

1.3. Fischer-Tropsch Synthesis

FTS is a process that converts syngas into a wide range of hydrocarbons with the help of a catalyst. The C-O bond is broken, allowing the carbon and hydrogen to react with molecular hydrogen, that results in the formation of hydrocarbons, water and, in a lesser extent, carbon dioxide. The product distribution of FTS follows a recognizable pattern, with the possible reactions happening in function of the CO:H_2 ratio of the syngas [27], [36]–[44].

$$n\mathrm{CO} + 2n\mathrm{H_2} \rightarrow \mathrm{C}_n\mathrm{H}_{2n} + n\mathrm{H_2O} \quad (6)$$

$$n\mathrm{CO} + (2n+1)\mathrm{H_2} \rightarrow \mathrm{C}_n\mathrm{H}_{2n+2} + n\mathrm{H_2O} \quad (7)$$

For CH_4 production, the syngas entering the FTS chamber must have a ratio of CO:H of 3:1 to guarantee the highest selectivity for CH_4 production[36], [38], [44]. The methanation process by FTS is shown in Figure I.3.

The prime catalysts for FTS are Fe, Co, Ni, Ru, with only Fe and Co being used in

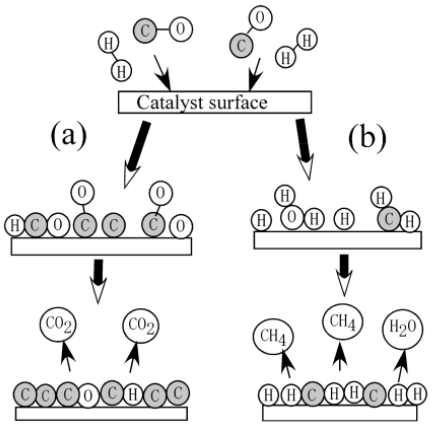

Figure I.3 - FTS reaction steps. Adapted from [34].

commercial applications. Ru is not commonly used despite being the most active due to its scarcity and high price. Ni, on the other hand, is neglected for its low catalyst capabilities of producing long chains of hydrocarbons, although it has a high selectivity for methane production [40], [41], [43], [45]. Fe and Co can operate stably under optimized conditions. Nevertheless, when in disfavourable operation conditions – high temperature and flow rate – Fe is more advantageous due to its higher resistance against operational poisons, e.g. halogenated compounds. By contrast, Co has a longer lifetime than Fe and is more active at low temperatures, but needs a cleaner syngas (its more susceptible to poisons) [36], [39], [43]. Finally, Fe has positive effect on the reaction rate with increasing CO partial pressure, whilst other catalysts are not influenced by this parameter [40], [43].

FTS product distribution is sensitive to pressure and temperature, since the FTS reaction is strongly exothermic, generating around 150 kJ/mole of converted CO_2. Therefore, it is necessary to precisely control temperature and heat exchanges, with the goal of maximizing the desired products and maintain catalyst stability. As such, there are two main operating temperature classes for FT reactors: High-Temperature FTS (HTFTS) reactors and Low-Temperature FTS (LTFTS) reactors [36], [38], [40].

LTFTS reactors work in the range of 180-250 ºC and are capable of synthesis of long-chain hydrocarbons waxes and paraffins. This process is employed in the synthesis of high-quality sulfur-free diesel fuels. Fe and Co are the catalyst of choice here, with Co performing better for lower temperatures [36], [37], [40].

HTFTS reactors operate in the range of 300-350 ºC, mainly producing light hydrocarbons in the gas phase. This process is best suited to produce gasoline. The extraction of chemicals is also possible, thanks to the high selectivity towards linear 1-olefins and oxygenates permits the extraction of chemicals. Since it operates at high temperatures, the preferred catalysts are iron-based [36], [37], [40].

II. Model Description

All the results obtained in this work were simulated by modelling the electrolysis and FTS process, from their kinetic reactions. A kinetic model consists in a mathematical representation of how a reaction evolves through time as a function of the system's components.

2.1. Electrolysis

In the process of electrolysis, the global equation that describes the charge-transfer kinetics occurring at the anode and the cathode is the Butler-Volmer equation (eq.8) [10], [25],

$$j = j_0 \left(\exp\left(\frac{\alpha_a F \left(v - \eta - E^0\right)}{RT}\right) - \exp\left(\frac{\alpha_c F \left(v - \eta - E^0\right)}{RT}\right) \right) \quad (8)$$

Where j is the reaction current density, j_0 is the exchange-current density, v is the applied voltage, α_a and α_c are the anodic and cathodic transfer coefficients, which are a characteristic of the electrodes used, η is the overpotential, E^0 is the equilibrium potential in standard conditions, F is Faraday's constant, R is the ideal gas constant and T is the temperature. Solving the Butler-Volmer equation in function of the applied potential on the electrodes allows the tracing of a JV curve of the electrochemical cell. The overpotential used here encapsulates all the different overpotentials that affect the reactions, in order to simplify the model.

The energy and faradaic efficiencies of the EC are also important parameters, which are given by the following equations [6], [10]:

$$\text{E.E.} = \frac{\text{E}^0}{\text{E}^0 + \eta} e_f \quad (9)$$

Where E.E is the energy efficiency and e_f is the faradaic efficiency. Energy efficiency is the ratio between the energy contained in the products and the electrical energy applied, whereas the faradaic efficiency is the fraction of the charge provided that was utilized in the reaction. The faradaic efficiencies used in this work are based of the common values found on literature, which are around 100% for CO production and 80% for methanation [6], [10], [24], [46].

The quantity of product being generated in the EC by time is defined by Equation

(10) [6], [10],

$$m_i = \frac{Q}{n_i F} \text{E.E.} \tag{10}$$

where m_i represents the number of moles of specie *i* generated, n_i is number of electrons transferred per molecule of product and Q the total charge.

2.2. Fischer-Tropsch Synthesis

FTS modelling is a widely researched subject leading to many proposed rate equations to describe the process. In 2015, Mousavi et al. [43] did a comprehensive study of all the proposed mechanisms and equation for cobalt and iron based FTS, arriving at a rate equation that best describes the process, presented here as Equation 11.

$$r_b = A \cdot \frac{P_{H_2}^{0.75} \cdot P_{CO}}{(1 + k_b \cdot P_{CO})^2} \tag{11}$$

In the rate equation, proposed by Mousavi et al. (2015), r_b is the reaction rate for the catalyst *b* (cobalt or iron), P_{H2} and P_{CO} are the partial pressures of H_2 and CO, respectively, k_b is the adsorption coefficient of CO and A is a rate constant. This latter parameter is only valid for temperatures of 533K, being a LTFT process.

Since nickel is a highly selective catalyst for methane production, Rönsch et al. [47] developed rate equations for FTS methanation using commercial catalysts with 18% and 50% of nickel. The rate equations proposed by Rönsch et al. (2015) are the following:

$$r_{18\%Ni} = -\frac{k_{1,18\%Ni} K_C K_H^2 P_{CO}^{0.5} P_{H_2}}{(1 + K_C P_{CO}^{0.5} + K_H P_{H_2}^{0.5})^3} \tag{12}$$

$$r_{50\%Ni} = -\frac{k_{1,50\%Ni} K_C K_H^2 P_{CO}^{0.5} P_{H_2}}{(1 + K_C P_{CO}^{0.5} + K_H P_{H_2}^{0.5})^3} \tag{13}$$

Where $k_{1,18\%Ni}$ and $k_{1,\ 50\%Ni}$ are the rate coefficients for CO methanation and $K_{C/H}$ are the adsorption constants for C and H, respectively.

III. Results and Discussion

In this chapter, the results of the simulation studies are presented and analyzed to evaluate both 1-step and 2-step solar-to-methane production approaches shown in Figure I.1.

3.1. Electrolysis

To simulate the electrolysis, a description of the electrochemical processes of the two methanation methods is necessary. Figure III.1 represents the electrochemical systems for direct methanation (route (a) in Figure I.1) and syngas (route (b) in Figure I.1) production, respectively.

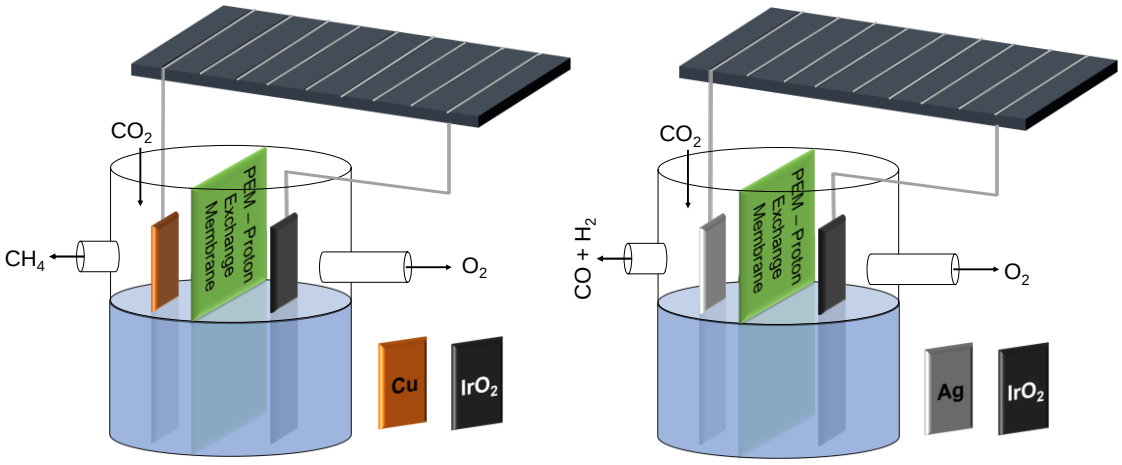

Figure III.1 – Electrochemical systems considered for direct methanation (1-step process) on the left, and for syngas production (2-step process) on the right.

An Ag electrode was considered for syngas and Cu for methane production. In the center of the ECs, a proton exchange membrane (PEM) is used to separate the anode from the cathode and to facilitate the separation of the cathodic and anodic reaction products [2], [6], [10]. This membrane only allows H^+ to pass through it, maintaining the cathodic and anodic reaction products separated. Various simulations were made whilst changing the ratios between the areas of PV and electrodes and the best results were obtained when the area of the electrodes is 10 % of the area of PV. With a smaller percentage, the current in the electrodes could not match the PV current (the electrochemical and the PV IV curves did not intercept) and with

bigger percentages the electrochemical cell was operating in a less than ideal zone of its electrochemical curve (in an unstable zone of the electrochemical IV curve). In relation to the CO_2 in the cell, a constant overflow of CO_2 is considered to eliminate it as a limiting factor, in order to calculate the maximum output of the electrochemical devices because for every mol of hydrocarbon produced, the same amount of CO_2 is spent, following the reaction stoichiometry. The EC works at ambient temperature (25 ºC), and the PV system powering the EC is built with modules made of the commercial mono crystalline silicon solar cell *Sunpower™ B50* [48]. A commercial solar cell was chosen instead of simulating a brand new in order to ground the simulation in reality. All the assumptions made for the ECs are then the following:

- Constant overflow of CO_2;
- Ambient temperature (25º C);
- Area PV:Area EC ratio of 10:1;
- Cu cathode for methanation and Ag cathode for syngas production;
- IrO_2 anode for both ECs;
- Commercial mono crystalline silicon solar cell *Sunpower™ B50* for powering the ECs;
- PEM used to facilitate the product removal.

3.1.1. Description of the PV system

As mentioned in the previous section, the building block of the PV system is a commercial mono-crystalline silicon solar cell (*Sunpower™ B50*). The characteristics of this commercial cell are presented on Table III.1, where P_{mpp}, V_{mpp} and I_{mpp} are the power, voltage and current, respectively, for the maximum power point of the cell, V_{oc} is the open circuit voltage and I_{sc} is the short circuit current. In Figure III.2 an image of the solar cell and its IV curves for different irradiations are presented [48].

This solar cell is endowed with an interdigitated all-back contact design, superior temperature performance, lack of light-induced degradation and broad spectral response. Such attributes make it highly efficient and one of the top-in-the-market silicon-based solar cells [48]. Thus, it was chosen to be the PV building block for this work.

Table III.1 – Characteristics of the Sunpower™ B50 solar cell @ Standard Test Conditions (STC) (1000 W/m^2, AM 1.5G and cell temperature of 25 ºC) [48].

Pmpp (Wp)	3.15
Efficiency (%)	21.2
Vmpp (V)	0.571
Impp (A)	5.51
Voc (V)	0.673
Isc (A)	5.87
Area (cm²)	156.25

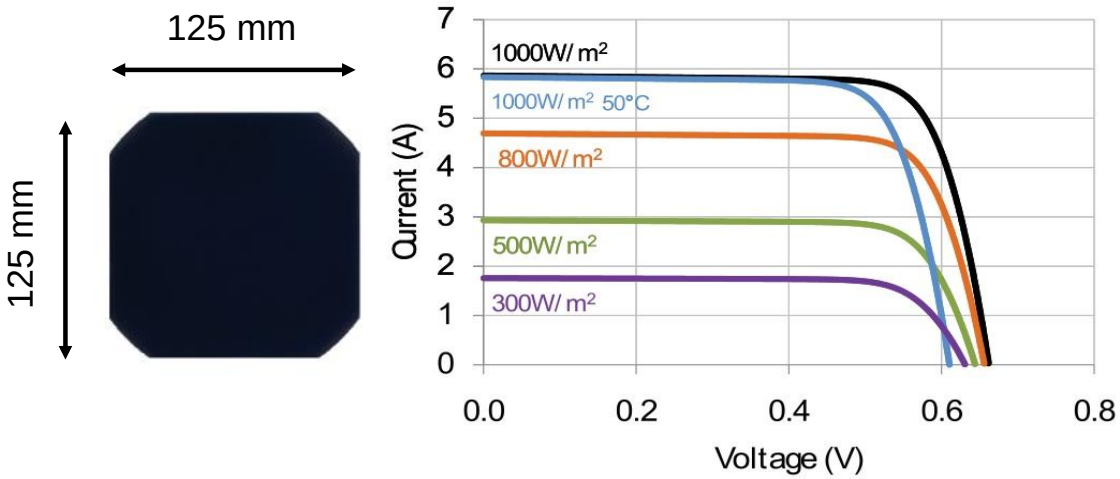

Figure III.2 – On the left, picture of the Sunpower™ B50 solar cell and, on the right, its IV responses for different irradiations and temperature [48]. There are no bus bars visible on the solar cell front due to its interdigitated back contact (IBC) configuration.

As solar energy is an intermittent source of energy, its direct use and storage proves difficult. So, there is currently the need to compensate the energy fluctuations to the grid via thermal generation, usually provided by fossil fuel combustion. Using solar energy as a means to produce clean hydrocarbons, as methane, this intermittency problem is resolved, creating a robust and carbon-neutral storage system [2], [15].

3.1.2. Simulation of the electrochemical IV curves

From the Butler-Volmer equation (Equation 8), the EC characteristic curve (IV) can be obtained by establishing the value of the parameters involved. While temperature, Faraday's and ideal gas constants are known parameters, the overpotential (η), the exchange-current density (J_0) and the anodic/cathodic transfer coefficients ($\alpha_{a/c}$) need to be simulated. To find these parameters, the electrochemical curve was simulated against experimental curves from the works of Singh, Clark and Bell (2015), that were obtained using the same electrodes and basis conditions [49]. In Figure III.3, it is represented the best simulated approximation of the experimental data for the cathode reaction.

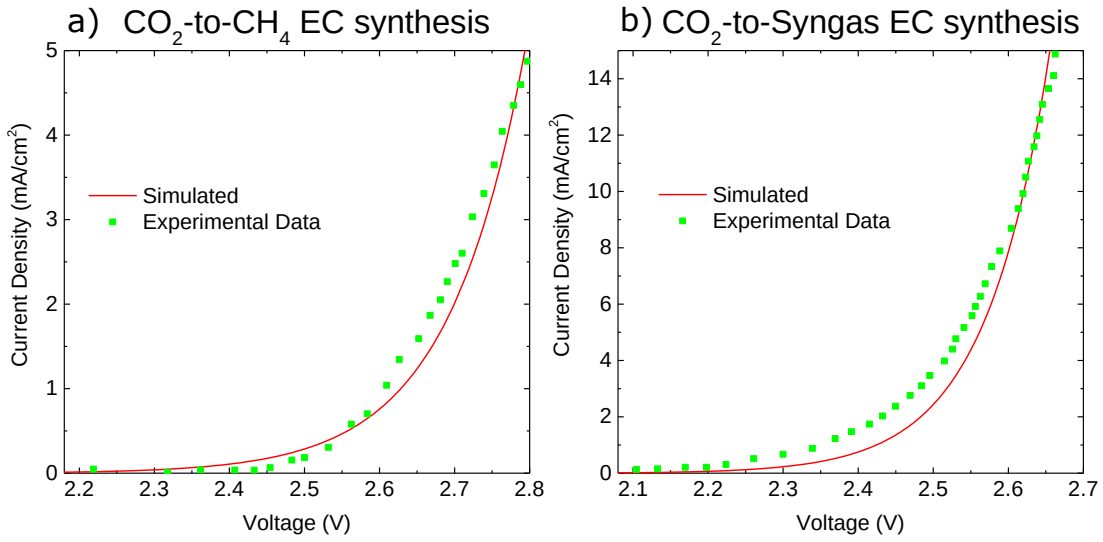

Figure III.3 - Comparison between the simulated (red) and the experimental (green) cathodic current densities for a) the direct methanation and b) the syngas production. Experimental cathodic current densities extracted from [49].

Analyzing both curves in Figure III.3, a close match is almost achieved between simulated and experimental curves. The discrepancies are due to the fact that this a process with many hidden variables, of which not all are considered in this study. Nevertheless, the simulated curve is a close approximation to the real one, allowing to infer the previous unknown parameters. It can be observed that the electrochemical reaction for direct methanation needs a higher voltage (2.4 V) to start than the reduction reaction of CO_2 into CO (2.2 V), as previously referred in Introduction [1], [3]–[4], [7]–[9], [13]–[15], [17], [37]–[38]. All the parameters used in this simulation are shown in Table III.2. It is verified that there is a

substantialy higher exchange-current density in the 2-step process. J_0 represents the balanced Faradaic current at equilibrium, i.e. the residual current when there is no aplied potential. The lower this exchange-current is, the larger the overpotential is, resulting in a sluggish reaction [10], [19], [25], [51]. Consequently, the 1-Step process has a slower, less efficient reaction, that can be atributed to its higher number of substeps (8 electronic exchanges as compared with only 2 for syngas production).

The transfer coefficients ($\alpha_{a/c}$) are the fraction between the polarization change in the anode and the cathode, that are intimately tied with the reaction rate. As both processes occur in the cathode, while oxygen evolution occurs in the anode, the tranfer coefficients referring to the anode are null. The slightly higher transfer coefficient, for the CO production step, is once more in line with the rest of the inferences made previously, which are supported by the literature [1], [6], [10], [15], [17], [18], [25], [51].

Table III.2- EC parameters for modelling direct methanation (1-step) and syngas production (2-step).

Parameter	**1-step**	**2-step**
E_0 (V)	1.06 [6]	1.34 [6]
J_0 (mA/cm²)	1.5×10^{-3}	8×10^{-3}
α_a	0	0
α_c	0.3	0.25
η (V)	0.9	0.67
F (C/mol)	96487 [10]	
R (J/mol.K)	8.314 [10]	
T (K)	298.15	

From the overpotential, it is possible to calculate the efficiency for both processes. Common values for Faradaic efficiencies are around 100% for CO production and

80% for methanation [6], [10], [24], [46]. Therefore, the energy efficiencies for direct methanation and syngas production are 43.3 % and 66.7 % (Equation 9), respectively. A better understanding of the electrochemical reactions mechanisms of both processes is needed to increase these efficiencies.

3.1.3. Electrolysis Temperature Dependence

This electrochemical system is being designed to operate at ambient temperature, without a need for temperature control. However, different regions in the world have different ambient temperatures, meaning that 298.15 K (25 ºC) is not valid everywhere. One other possibility, already studied for photoelectrochemical devices [20], is the use of a compact PV-EC device. This device would operate at higher temperatures than the ambient one, since the PV components would release heat to the EC. Thus, a study on how temperature affects the electrochemical reaction was conducted in order to determine if such device could be applicable in this technology. In Figure III.4 are presented IV curves at different temperatures for both electrochemical processes.

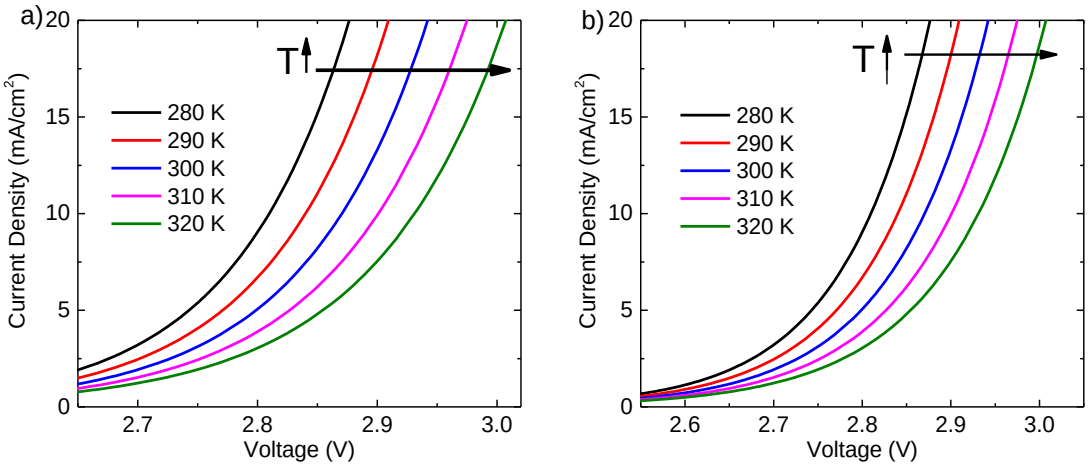

Figure III.4 - Temperature dependence of the electrochemical curves for a) direct methanation and b) syngas production.

Observing the curves shown in Figure III.4, it is evident a shift to higher voltages with the increase of temperature. This shift represents an increase of 0.003 V/K, which is a small value and, thus, it is needed big temperature fluctuation, in the order of hundreds of kelvins, to disrupt in a meaningful manner the performance of the electrochemical cells. This indicates a small drop in efficiency at higher temperatures and shows that lower temperature is conducive to the electrochemical reduction of

CO_2. This trend is actually opposite to what is expected in literature, with ECs performance increasing with temperature[2], [8], [20], [21], [52], [53]. This shows a limitation of this model and means that is only usable for modelling electrochemical reactions at 25 ºC. A better, more advanced model is needed to evaluate the evolution of ECs with temperature, adding a thermal model as done by Olivier et al. (2016) [52].

3.1.4. Determination of the operation voltage and current

The calculation of the production rate of the ECs requires the definition of the operation voltage and current. These parameters are given by the intersection between the PV's and the EC's I-V curves, which should ideally occur at the maximum power point of the PV cell (i.e. at V_{mpp} and I_{mpp}) to operate with minimum energy losses [18]. This intersection is shown in Figure III.6. As will be mentioned later, a high operation voltage is necessary and, consequently, a custom-built solar module will be employed. So, utilizing the *Sunpower™ B50* solar cells as the base units for the PV modules, it was calculated that a module consisting of five of such in series is the best for driving the electrochemical reactions for both processes.

A total active PV area of 781.25 cm^2 was considered. For a module with 5 series-connected solar cells, the operating point for direct methanation is 2.58 V and 5.69 A and the operating point for syngas production is 2.38 V and 5.78 A. In Figure III.5 is presented this PV configuration. This module was chosen since it presents the best operating point for both processes. The operating point is ideal in the maximum power point of the PV system. It can be seen that for the direct methanation process, the operation point is closer to the maximum power point than in the syngas production process, meaning that it can operate closer to the ideal of the PV system. This then translates into an hourly production 2 g/h of carbon monoxide and 0.15 g/h of molecular hydrogen for syngas production. Therefore, to estimate production in function of PV area, the previous calculations were done while considering more parallel-connected PV modules, which will increase the overall current of the system. In Figure III.7 are shown the curves for 5, 10, 25 and 50 parallel connected modules. In Table III.3 and Table III.4 are shown the results of those calculations for the methanation and the syngas production, respectively, and in Table III.5 are summarized the volume of methane and syngas produced in the ECs in function of the area of PV and time.

Figure III.5 – Representation of the basic module of the PV system, consisting of five *Sunpower™ B50* solar cells in series.

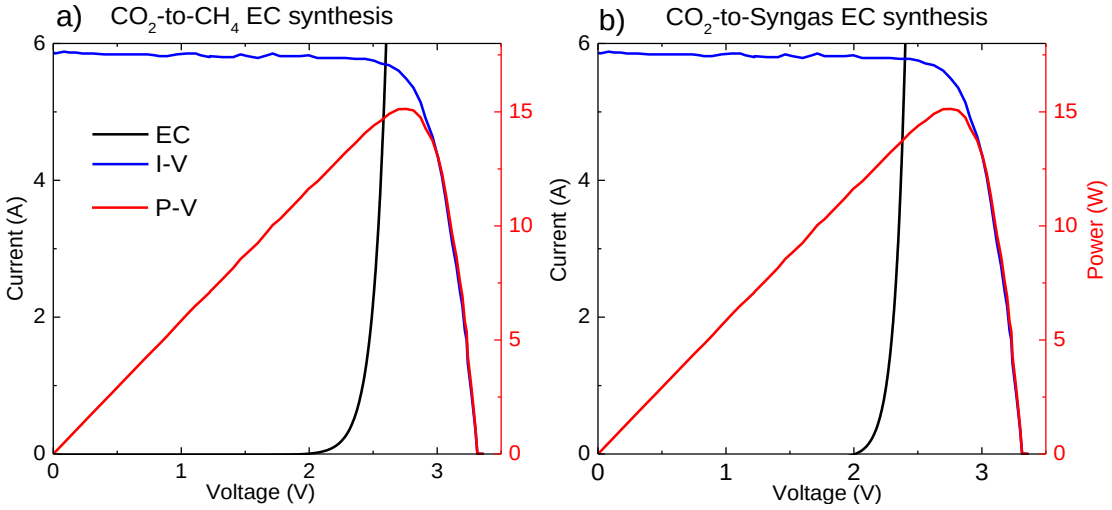

Figure III.6 – I-V and power-voltage (P-V) curves of the basic PV module shown in Figure III.5, overlaid with the electrochemical curve of a) methanation and b) syngas synthesis, where in blue are represented the solar cell I-V curve, in black the EC IV curve and in red the solar P-V curve.

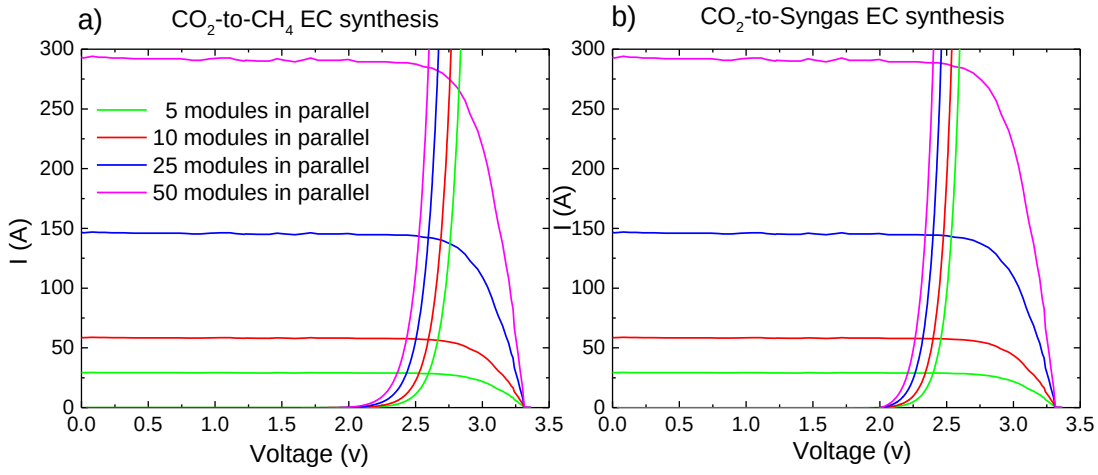

Figure III.7 . The I-V curves of different PV sources composed of distinct number of parallel-connected modules as that of Figure III.5, in order to add their current, overlaid with the electrochemical load curves of a) methanation and b) syngas synthesis for 5, 10, 25 and 50 parallel modules.

It is notable a higher production of syngas by CO_2 reduction when compared to the much modest production of CH_4 by CO_2 direct methanation. This results from the, already mentioned in Introduction, higher efficiency and yield that syngas production presents and comes to strengthen the previous observation of being a faster reaction than methanation. It is observable in all curves that the direct methanation process occurs very closely to the maximum power point of the solar modules, which indicates a better solar to electrochemical efficiency in this process. In the case of syngas production, the PV system is not optimized for this electrochemical reaction, as the intersection does not occur at the maximum power point. Thus, it should be noted that with an optimized PV system the overall performance of PV-EC system would improve. However, note that syngas is just an intermediate fuel in route b) of Fig. I1, still requiring the subsequent FTS process to form CH_4.

Table III.3 – Performance of the 1-step process with increasing PV area.

No. Of Parallel modules	**V_{op} (V)**	**I_{op} (A)**	**Volume of CH_4 per hour (L/h)**	**Area of PV (cm^2)**
1	2.80	5.70	0.26	781.25
2	2.89	11.50	0.52	1562.50
3	2.91	17.25	0.78	2343.75
4	2.94	23.18	1.00	3125.00
5	2.97	28.85	1.30	3906.25
6	3.00	34.43	1.56	4687.50
7	3.02	40.23	1.82	5468.75
8	3.02	46.01	2.08	6250.00
9	3.04	51.60	2.33	7031.25
10	3.04	57.38	2.60	7812.50
15	2.86	86.24	3.90	11718.75
20	2.88	116.10	5.30	15625.00
30	2.93	173.37	7.80	23437.50
40	2.95	230.16	10.40	31250.00
50	2.98	288.00	13.00	39062.50

Table III.4 – Performance of the 2-step process with increasing PV area.

No. Of Parallel modules	V_{op} (V)	I_{op} (A)	Volume of CO per hour (L/h)	Volume of H_2 per hour (L/h)	Area of PV (cm^2)
1	2.58	5.74	1.60	1.69	781.25
2	2.64	11.30	3.21	3.38	1562.50
3	2.67	17.00	4.81	5.07	2343.75
4	2.68	22.50	6.46	6.81	3125.00
5	2.70	28.00	7.81	8.23	3906.25
6	2.73	33.38	9.31	9.81	4687.50
7	2.74	38.86	10.83	11.42	5468.75
8	2.75	44.12	12.30	12.97	6250.00
9	2.76	49.48	13.80	14.54	7031.25
10	2.76	55.00	15.33	16.16	7812.50
15	2.61	85.70	23.89	25.19	11718.75
20	2.64	113.60	31.67	33.39	15625.00
30	2.66	169.00	47.11	49.67	23437.50
40	2.70	224.20	62.50	65.90	31250.00
50	2.71	279.50	77.91	82.14	39062.50

Table III.5 - Production of the EC's for both processes per m^2 of active PV area.

Rate of production ($L/ h.m^2_{PV}$)	1-step	2-step
CH_4	3.3	-
CO	-	16
H_2	-	19

3.2. Fisher-Tropsch Synthesis

To complete the 2-step approach of Figure I.1, the produced syngas ($CO+H_2$) needs to be converted to methane in the second step of the process based on FTS. A simulation for each catalyst is made to evaluate which is preferred for the CH_4

production. The considered catalysts were Fe, Co and two Ni based (Ni/Al_2O_3) with a 18% and a 50% Ni concentration. To model these syntheses, two different kinetic models were considered. Firstly, a model for Fe and Co developed by Mousavi et al. (2015) and, secondly, a model for 18%Ni and 50% Ni developed by Rönsch et al. (2015). These syntheses occur at a temperature of 533 K (260 ºC), meaning they are low temperature FTS (LTFTS), since methane formation increases until it reaches a temperature around 600 K, when the reverse reaction, known as methane reforming, starts occurring, leading to a drop of the reaction rate [47]. Both kinetic models do not consider this factor, and thus, can only be used at temperatures below 600 K (see Annex I –Temperature Dependence for more information). In Equation (14) is presented the CO methanation reaction, that, as stated previously, is reversed when reached a certain temperature threshold.

$$CO + 3H_2 \rightleftharpoons CH_4 + H_2O \tag{14}$$

In order to form CH_4 by FTS, a 3:1 H_2:CO ratio is required, since other ratios will induce the formation of different hydrocarbons [36], [41], [43], [45], [54]. Although the 2-step EC produces, in volume, 16 $L/h.m^2_{PV}$ of CO and 19 $L/h.m^2_{PV}$ of H_2, to respect the ratio, only 6.3 of the 16 $L/h.m^2_{PV}$ of CO will be used in the synthesis, creating the need to store the remaining liters of CO being produced.

The reaction rates of both models show the rate of hydrocarbon formation, which is the same as the rate of CO consumed. Hence, the reaction rates are presented as negative, depicting the quantity of CO being consumed. This rate depends on the catalyst's surface area available, and consequently, on the quantity of catalyst on the reactor, on how swiftly the CO molecules adhere to the catalysts surface, on the partial pressure of syngas and the ratio between CO and H_2 and on the temperature.

The reaction rate of FTS is given in moles of CO consumed per kilogram of catalyst. For Mousavi's model, k_{Fe} and k_{Co} are known for iron and cobalt catalysts, obtained by modeling Equation (11) with experimental results, while A is a constant used to normalize the model. As of 2015, from all the proposed models for Co and Fe FTS , Mousavi's is regarded as the most reliable one [43]. As for Ni based FTS, Rönsch's model is the preferred one, with its rate coefficients, $k_{1,\ 18\%Ni}$ and $k_{1,\ 50\%Ni}$, are calculated by Equation (15) and the adsorption constants, K_C and K_H, by Equation (16) [47] :

$$k_{1,n} = k^0_{1,n} \exp\left(\frac{-A^0_n}{RT}\right) \tag{15}$$

$$K_j = K_j^0 \exp\left(\frac{-\Delta H_j^0}{RT}\right) \quad (16)$$

Where $k^0_{1,n}$ and K^0_j are the preexponential factor of rate coefficient for the catalyst *n* and of the adsorption constant for the adsorbed atom *j*, respectively. A^0 denotes the equilibrium potential and ΔH^0_j denotes the enthalpy of the adsorption reaction for the adsorbed atom *j*. The kinetic parameters for Equations (14) and (15) are given in Table III.6

Table III.6 - Kinetic parameters for Equations (15) and (16).

Preexponential factor of rate coefficient for 18 % Ni	$\mathbf{k^0_{1,18\%Ni}}$ **(mol/kg$_{cat}$.s)**	$4.2x10^9$
Preexponential factor of adsorption constant for 18 % Ni	$\mathbf{k^0_{1,50\%\ Ni}}$ **(mol/kg$_{cat}$.s)**	$5.3x10^9$
Preexponential factor of adsorption constant for 50 % Ni	$\mathbf{K^0_C}$ **(bar$^{-0.5}$)**	0.428
Preexponential factor of rate coefficient for 50 % Ni	$\mathbf{K^0_H}$ **bar$^{-0.5}$)**	0.165
Activation Energy	$\mathbf{A^0}$ **(J/mol)**	103000
Enthalpy of the adsorption reaction for carbon	$\mathbf{\Delta H^0_c}$ **(J/mol)**	-16000
Enthalpy of the adsorption reaction for hydrogen	$\mathbf{\Delta H^0_H}$ **(J/mol)**	-42000

The rate equations of FTS depend on partial pressure instead of volume. Therefore, they were solved for a CO partial pressure ranging between 0 and 20 bar, with the H_2 partial pressure three times the CO's. In Table III.7 are shown the parameters of Mousavi et al. (2015)'s model and in Table III.8 the ones given to the parameters of Rönsch et al. (2015)'s model. In Figure III.8 are the reaction rates for methanation using Fe, Co and Ni-based catalysts simulated via the aforementioned models.

Table III.7 – Parameters of Mousavi's Model.

A **(mol/Kg_{cat}.s)**	**k_{Fe}**	**k_{Co}**	**P_{H2}** **(bar)**
10^{-3} [43]	0.165 [43]	0.428 [43]	$3P_{CO}$

Table III.8– Parameters of Rönsch's Model.

K_c **(bar^{-1})**	**K_H** **(bar^{-1})**	**$k_{1,\ 18\%Ni}$** **(mol/Kg_{cat}.s)**	**$k_{1,\ 50\%Ni}$** **(mol/Kg_{cat}.s)**	**P_{H2}** **(bar)**
7.58	0.59	0.338	0.426	$3P_{CO}$

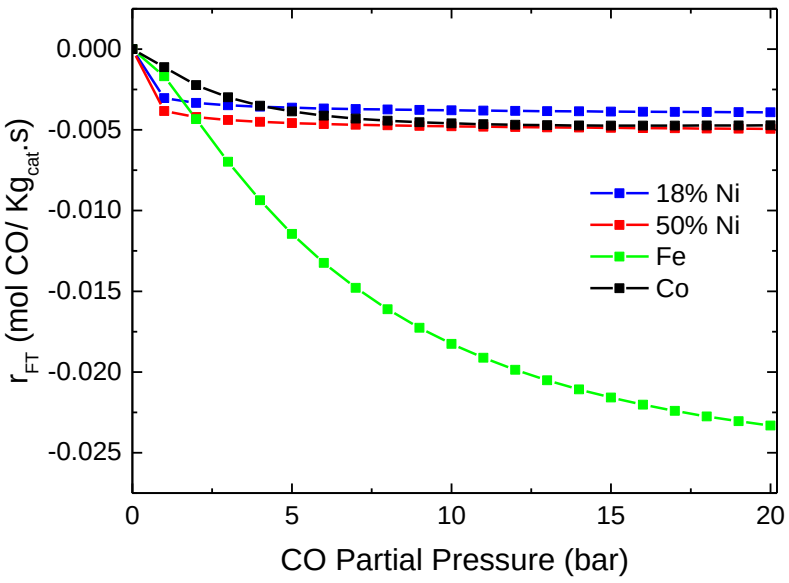

Figure III.8 - Reaction rates of CO methanation for different catalysts in function of CO partial pressure.

Analyzing the evolution of the FTS reaction rates with increasingly CO partial pressure, it is notable how only iron-based catalysts are sensible to the CO partial pressure whilst the rest with the catalysts the rate is almost constant. This behavior is expected, accordingly with literature [40], [43], and makes iron a very attractive catalyst, since it is also the least expensive of these catalysts [34], [36]. However, iron presents the lowest selectivity for methane, resulting in more unwanted hydrocarbons being produced alongside methane. For the remainder of this work, a CO partial pressure of 5 bar was considered, with the equivalent rates summarized

in Table III.9. Since the CO flow rate is 6.3 L/h.m^2_{PV}, it was calculated that, for each meter square of PV area used, 0.007 Kg of iron, 0.019 Kg of cobalt, 0.022 Kg of 15% nickel-based catalyst and 0.018 Kg of 50% nickel-based catalyst are necessary. This shows that not only is iron the cheapest catalysts, it is also the more efficient one.

Table III.9 – FTS reaction rates for P_{CO}=5 bar.

Catalyst	**r_{FT} (mol CO/Kg_{cat}.s)**	**r_{FT} (g CO/Kg_{cat}.s)**
Iron	-0.0114	-0.32
Cobalt	-0.0039	-0.11
15% Nickel	-0.0036	-0.10
50% Nickel	-0.0046	-0.13

3.2.1. Energy requirements for FTS

For efficient syngas-to-methane conversion, the syngas in the reactor for the FTS needs to be at a typical temperature around 533 K, , which constitutes the main energy consumption required in FTS. The energy required to heat up syngas to this temperature was calculated to better evaluate the overall energetic balance of the 2-step process. In Figure III.9 is shown a schematic of the heating process. For the calculations, it was considered a separation of the syngas into CO and H_2 and the subsequent heating of each gas separately. To calculate the necessary power to heat syngas from the input temperature (ambient temperature, 298 K) to the output temperature (533 K) it was used the following formula [55]:

$$h = \frac{q}{c_p \cdot \rho \cdot \Delta T} \tag{17}$$

Where h is heat flow rate in kW, q is the flow rate in m^3/s, c_p is the specific heat in kJ/kg.K, ρ is the density in kg/m^3 and ΔT is the temperature difference. All these parameters are presented in Table III.10. The flow rate for CO and H_2 are the

previously established 6.3 and 19 L/h.m^2_{PV}, respectively. These flow rates values were converted to $m^3/s.m^2_{PV}$ for these calculations.

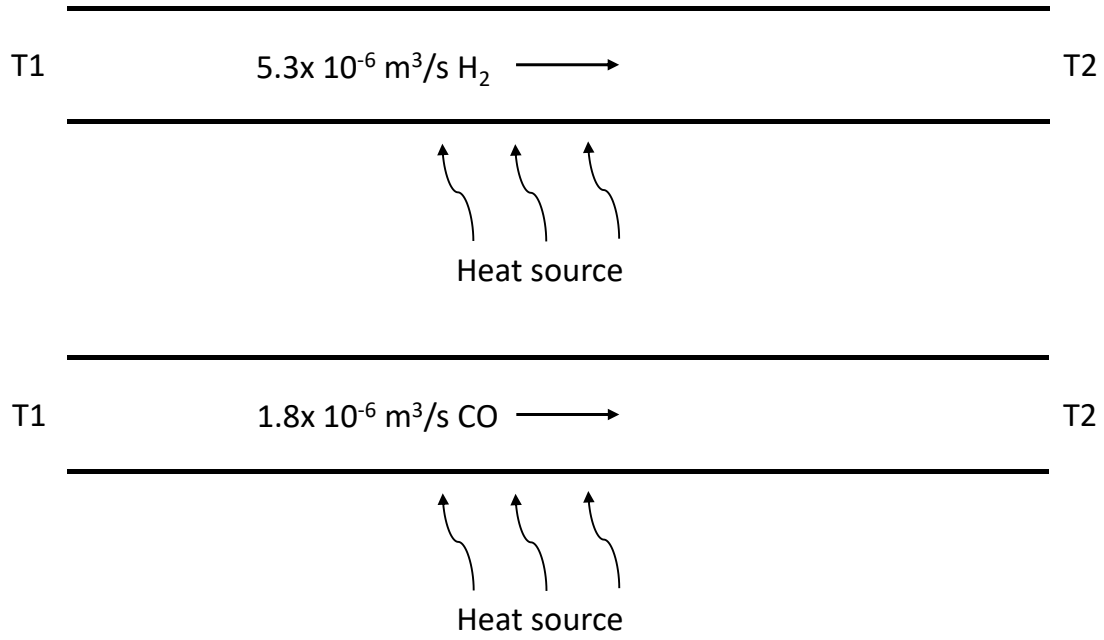

Figure III.9 – Heating process of syngas. T1 is the input temperature and T2 the output temperature. The input flow rates are those calculated from the EC production.

Table III.10 – Parameters for calculating the syngas heating power.

	q (m^3/s)	**c_p (kJ/kg.K)**	**ρ (kg/m^3)**	**ΔT (K)**
CO	$1.8x10^{-6}$	1.04	1.14	235
H_2	$5.3x10^{-6}$	14.3	$9x10^{-5}$	235

Solving Equation (17), it is calculated a needed potency of 0.5 W/m^2_{PV} for heating up the CO and a needed potency of 0.002 W/m^2_{PV} for heating up the H_2. These translate to a total energy requirement per m^2 of PV area of 2 Wh per day, assuming 4 sun peak hours daily as a yearly average for Europe [56].

3.3. 1-Step Methanation vs 2-Step Methanation

The previous results were compared in terms of energy, for an easier understanding of both processes, assuming CH_4 has an energy equivalent of 13.9 Wh/g [10]. For the 2-step process, the FTS energy requirement (calculated in section 3.2.1) was subtracted from the CH_4 energy equivalent in the following results. With these final values of production, it is also possible to calculate the overall solar-to-CH_4 efficiency. The results of the two processes are shown in Table III.11.

Table III.11 – Production of the 1- and 2-steps processes in volume and equivalent energy of CH_4.

	CH_4 produced per hour ($L/h.m^2_{pv}$)	**CH_4 energy equivalent per ($Wh/h.m^2_{pv}$)**	**EC efficiency (%)**	**Solar-to-CH_4 efficiency (%)**
1-step	3.3	30.14	43.3	9.18
2-step	6.3	55.53	66.7	13.63

It should be noted that, as mentioned in section 3.1.4, that syngas production with this PV-EC system is not working at the ideal operation point, which affects negatively its efficiency. These results assume the PV system is working at optimal conditions, always assuming a constant solar irradiance of 1000 W/m^2, which does not happen in reality. For a more realistic approach, global irradiance data from Ineichen (2011) [57] spanning one year is considered. This data was obtained using the highest measurement of the day in clear sky conditions. It was considered 4 sun peak hours daily. In Figure III.10, CH_4 adjusted production for a year is shown in terms of weight and equivalent energy. Analyzing this data, a higher performance in the summer is evident, which is explained by the higher solar irradiance during the summer period. It is once more observed the better performance of the 2-Step process. Lastly, the daily production average for both processes were calculated and the results are shown in Figure III.10.

Observing the results presented in Table III.12, it is verified that the 2-step approach production is almost twice the 1-step production. This process is the better one, suited for both small and large-scale applications, from domestic to industrial uses. In terms of the 1-step process, while it has lower efficiencies and methane rates, it is a simpler process, easily applicable in a household and totally self-sustained, not being indicated for large-scale applications.

Table III.12 - Average daily performance of the 1- and 2-steps processes in volume and equivalent energy of CH_4, considering 4 sun peak hours per day.

	Volume of CH_4 produced daily (L/m^2_{PV})	**CH_4 Energy equivalent daily (Wh/m^2_{PV})**
1-Step	15.24	69.58
2-Step	29.01	132.83

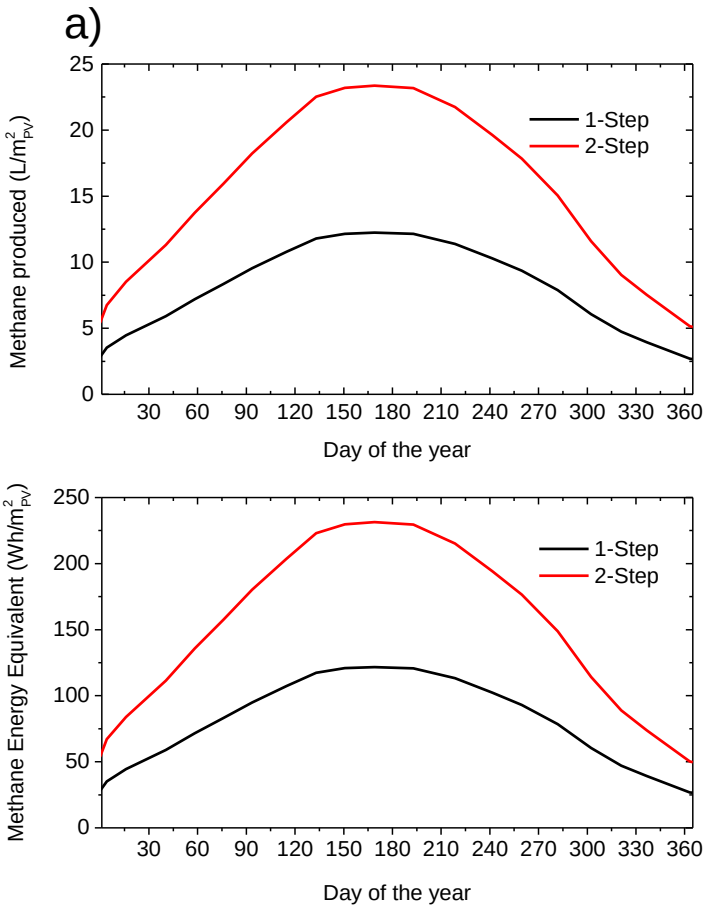

Figure III.10– Daily performances of both processes in a) volume of methane and b) methane energy equivalent.

3.4. Practical application

Taking into account the previous results, the performance of the two processes was analyzed with the goal of satisfying the heat requirements of a average European household. According to data from the 2018 report from BP on Statistical Review of World Energy [58], a European household consumes an average of 11630 kWh per year (31.86 kWh/day) of natural gas (CH_4). Knowing this, for these processes to power one of these households they would need a PV area of 86.8 and 58.4 m^2 for the 1-step and the 2-step, respectively, as indicated in Figure III.11. These values were calculated using the solar-to-CH_4 efficiencies shown in Table III.11, considering an average of 4 sun peak hours daily at a solar peak irradiance of 1 kW/m^2. This analysis shows that such PV systems could be installed on the available solar-exposed area on the roofs and/or facades of these households.

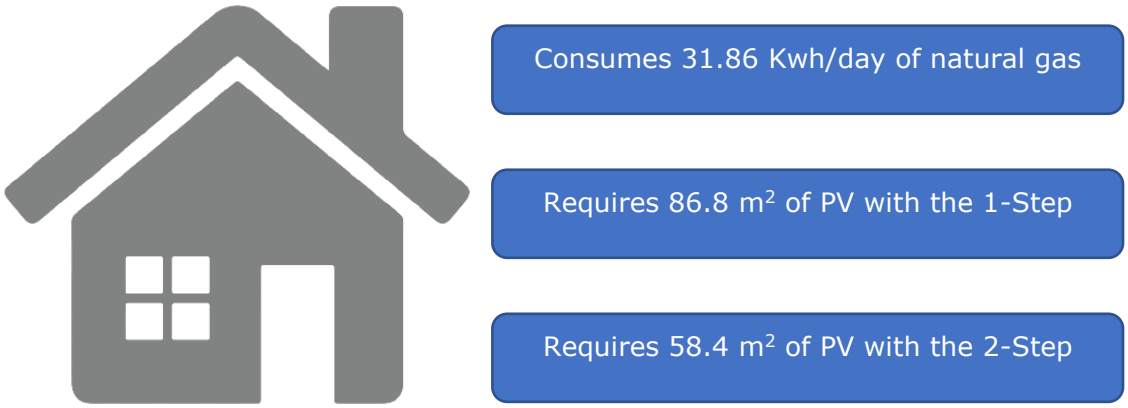

Figure III.11 - Requirements for powering up an average European household.

IV. Conclusion

In this work, two different approaches for CO_2 methanation were studied. The first, a 1-step approach, is an electrochemical conversion of CO_2 into CH_4 using water as a proton donor, powered by clean energy harvested from the sun. The second, 2-step approach, is the co-electrolysis of CO_2 and water into syngas that is then used as feedstock for a Fischer-Tropsch synthesis, producing methane. To evaluate both approaches, they were simulated using kinetics-based models.

From the simulation of the electrochemical reactions, it was concluded that the 2-step electrochemical process is a quicker and more efficient process than the 1-step, with the former producing 20.01 $g/h.m^2_{PV}$ of CO and 1.71 $g/h.m^2_{PV}$ of H_2 with a total energy efficiency of 66.6 %, while the latter produced 2.17 $g/h.m^2_{PV}$ with a total electrochemical energy efficiency of 43.3 %. It should be noted that the 2-step process is more efficient even though its less optimized PV-EC system.

Four FTS catalysts were simulated, with iron rising above the others performance-wise. Although this catalyst has the smallest selectivity for CH_4 formation (~70%), due to its low price and a high reaction rate, it was the preferred one [40].

Analyzing the overall efficiency, from the harvesting of solar energy by the photovoltaic system to the volume of CH_4 produced, the solar-to-CH_4 efficiencies are 9.18 % for the 1-step process and 13.63 % for the 2-step process. The main limitation for these efficiencies is the efficiency of the PV system, that is 21.2 %. Thus, with the rising of more efficient PV technologies, this overall efficiency will grow too.

Before analyzing the practicality of both methanation systems, it should be pointed out that we are dealing with low maturity stage technologies and that breakthrough developments may radically change the performance of both systems. A substantial research effort is still necessary before these technologies can be used commercially. This work points out the high energy efficiency of the electrochemical syngas production process. This step, coupled to new developments in catalysts for the FTS step that will allow carrying out methanation at lower temperatures together with innovations in reactor design, shows its high potential for small- and large-scale applications. However, the 1-step system, being a simple process that works near room temperature, has the potential of becoming very cost-efficient and is especially suited for small scale projects, by powering of private residencies alongside other clean energies, as a means to decrease dependency on fossil energy.

4.1. Future Perspectives

It should be noted that the model here presented is very limited, only based on the basic kinetic processes of electrolysis. It was designed to comprehend the potentialities of the processes study and give an idea of the path to follow in future studies. In follow up works, this model should be put to test with experimental work, to more closely confirm their efficacy and should be completed to include the whole system (auxiliary systems, e.g. pumps, valves, heating and cooling units etc.) behavior. The model should also be made more complete by adding thermodynamic considerations to it.

Experimental work based on the findings of this model has to be done, to confirm the findings for large areas of PV and stress studies should be done to verify how performance is affected with increasing operation times.

Finally, studies on the impact of nanopatternization of the electrodes should be done. Nanopatterning of electrodes or even the use of nanoparticles as the electrodes is a new study subject that has been getting popular in the last few years and shows great promise in the improvement of electrochemical processes, bringing them closer to viable use.

Bibliography

[1] J. A. Herron, J. Kim, A. A. Upadhye, G. W. Huber, and C. T. Maravelias, "A general framework for the assessment of solar fuel technologies," *Energy Environ. Sci.*, vol. 8, no. 1, pp. 126–157, 2015.

[2] G. Ibram, "Solar fuels vis-à-vis electricity generation from sunlight: The current state-of-the-art (a review)," *Renew. Sustain. Energy Rev.*, vol. 44, pp. 904–932, 2015.

[3] C. Graves, S. D. Ebbesen, and M. Mogensen, "Co-electrolysis of CO2 and H2O in solid oxide cells: Performance and durability," *Solid State Ionics*, vol. 192, no. 1, pp. 398–403, 2011.

[4] M. Schreier, L. Curvat, F. Giordano, L. Steier, A. Abate, S. M. Zakeeruddin, J. Luo, M. T. Mayer and M. Grätzel "Efficient photosynthesis of carbon monoxide from CO2 using perovskite photovoltaics," *Nat. Commun.*, vol. 6, p. 7326, 2015.

[5] M. Samavati, M. Santarelli, A. Martin, and V. Nemanova, "Production of Synthetic Fischer-Tropsch Diesel from Renewables: Thermoeconomic and Environmental Analysis," *Energy and Fuels*, vol. 32, no. 2, pp. 1744–1753, 2018.

[6] A. J. Martín, G. O. Larrazábal, and J. Pérez-Ramírez, "Towards sustainable fuels and chemicals through the electrochemical reduction of CO_2: lessons from water electrolysis," *Green Chem.*, vol. 17, no. 12, pp. 5114–5130, 2015.

[7] A. Tatin, C. Comminges, B. Kokoh, C. Costentin, M. Robert, and J.-M. Savéant, "Efficient electrolyzer for CO_2 splitting in neutral water using earth-abundant materials," *Proc. Natl. Acad. Sci.*, vol. 113, no. 20, pp. 5526–5529, 2016.

[8] S. Fukuzumi, "Production of Liquid Solar Fuels and Their Use in Fuel Cells," *Joule*, vol. 1, no. 4, pp. 689–738, 2017.

[9] B. Endrődi, G. Bencsik, F. Darvas, R. Jones, K. Rajeshwar, and C. Janáky, "Continuous-flow electroreduction of carbon dioxide," *Prog. Energy Combust. Sci.*, vol. 62, pp. 133–154, 2017.

[10] J. Newman and K. Thomas-Alyea, *Electrochemical Systems*, 3rd ed. John Wiley & Sons, 2004.

[11] W.-H. Cheng, M. H. Richter, M. M. May, J. Ohlmann, D. Lackner, F. Dimroth, T. Hannappel, H. A. Atwater and H. Lewerenz, "Monolithic Photoelectrochemical Device for Direct Water Splitting with 19% Efficiency," *ACS Energy Lett.*, vol. 3, no. 8, pp. 1795–1800, Aug. 2018.

[12] T. Hatsukade, K. P. Kuhl, E. R. Cave, D. N. Abram, and T. F. Jaramillo, "Insights into the electrocatalytic reduction of CO_2 on metallic silver surfaces," *Phys. Chem. Chem. Phys.*, vol. 16, no. 27, pp. 13814–13819, 2014.

[13] J. L. White, J. T. Herb, J. J. Kaczur, P. W. Majsztrik, and A. B. Bocarsly, "Photons to formate: Efficient electrochemical solar energy conversion via reduction of carbon dioxide," *J. CO2 Util.*, vol. 7, pp. 1–5, 2014.

[14] C.R. Graves, "Recycling CO2 into Sustainable Hydrocarbon Fuels: Electrolysis of CO2 and H2O." Columbia University, 2010. 245 p.

[15] H. L. Tuller, "Solar to fuels conversion technologies: A perspective," *Mater. Renew. Sustain. Energy*, vol. 6, no. 1, 2017.

[16] J. Qiao, Y. Liu, F. Hong, and J. Zhang, "A review of catalysts for the electroreduction of carbon dioxide to produce low-carbon fuels," *Chem. Soc. Rev.*, vol. 43, no. 2, pp. 631–675, 2014.

[17] M. Gattrell, N. Gupta, and A. Co, "A review of the aqueous electrochemical reduction of CO2to hydrocarbons at copper," *J. Electroanal. Chem.*, vol. 594, no. 1, pp. 1–19, 2006.

[18] M. Schreier, L. Curvat, F. Giordano, L. Steier, A. Abate, S. M. Zakeeruddin, J. Luo, M. T. Mayer and M. Grätzel "Efficient photosynthesis of carbon monoxide from CO2 using perovskite photovoltaics," *Nat. Commun.*, vol. 6, p. 7326, 2015.

[19] K. Manthiram, B. J. Beberwyck, and A. P. Alivisatos, "Enhanced electrochemical methanation of carbon dioxide with a dispersible nanoscale copper catalyst," *J. Am. Chem. Soc.*, vol. 136, no. 38, pp. 13319–13325, 2014.

[20] K. Welter, V. Smirnov, J. P. Becker, P. Borowski, S. Hoch, A. Maljusch, W. Jaegermann and F. Finger "The Influence of Operation Temperature and Variations of the Illumination on the Performance of Integrated Photoelectrochemical Water-Splitting Devices," *ChemElectroChem*, vol. 4, no. 8, pp. 2099–2108, 2017.

[21] A. Buttler and H. Spliethoff, "Current status of water electrolysis for energy storage, grid balancing and sector coupling via power-to-gas and power-to-liquids: A review," *Renew. Sustain. Energy Rev.*, vol. 82, no. February 2017, pp. 2440–2454, 2018.

[22] M. Shen, N. Bennett, Y. Ding, and K. Scott, "A concise model for evaluating water electrolysis," *Int. J. Hydrogen Energy*, vol. 36, no. 22, pp. 14335–14341, 2011.

[23] J. Qiao, Y. Liu, and J. Zhan, *Electrochemical Reduction of Carbon Dioxide. Fundamentals and Technologies*, 1st Editio. CRC Press, 2016.

[24] P. Yadav and S. Basu, "An Integrated Device for Converting Water, Carbon Dioxide and Light into Electricity and Organics," *J. Electrochem. Soc.*, vol. 164, no. 11, pp. E3406–E3417, 2017.

[25] M. R. Singh, E. L. Clark, and A. T. Bell, "Effects of electrolyte, catalyst, and membrane composition and operating conditions on the performance of solar-driven electrochemical reduction of carbon dioxide," *Phys. Chem. Chem. Phys.*, vol. 17, no. 29, pp. 18924–18936, 2015.

[26] T. Pardal, S. Messias, M. Sousa, A. S. R. Machado, C. M. Rangel, D. Nunes, J. V. Pinto, R. Martins and M. N. Ponte "Syngas production by electrochemical CO2reduction in an ionic liquid based-electrolyte," *J. CO2 Util.*, vol. 18, pp. 62–72, 2017.

[27] Y. Redissi and C. Bouallou, "Valorization of carbon dioxide by co-electrolysis of CO2/H2O at high temperature for syngas production," *Energy Procedia*, vol. 37, pp. 6667–6678, 2013.

[28] T. Pardal, T. R. C. Fernandes, A. S. R. Machado, and C. M. Rangel, "Conversion of Carbon Dioxide into Fuel by Electrochemical Reduction In Aqueous Solvents," *Fuel Cells Adv. Batter.*, vol. 2, no. 9, pp. 26–28, 2013.

[29] M. R. Singh, E. L. Clark, and A. T. Bell, "Thermodynamic and achievable efficiencies for solar-driven electrochemical reduction of carbon dioxide to transportation fuels," *Proc. Natl. Acad. Sci.*, vol. 112, no. 45, pp. E6111–E6118, 2015.

[30] H. S. Jeon, J. Koh, S. Park and M. S. Jee "A monolithic and standalone solar-fuel device having comparable efficiency to photosynthesis in nature," *J. Mater. Chem. A*, vol. 3, no. 11, pp. 5835–5842, 2015.

[31] M. Ma, K. Liu, J. Shen, R. Kas, and W. A. Smith, "In-situ Fabrication and Reactivation of Highly Selective and Stable Ag Catalysts for Electrochemical CO2 Conversion," *ACS Energy Lett.*, p. acsenergylett.8b00472, 2018.

[32] M. Bevilacqua, J. *Filippi and M. Folliero*, "Enhancement of the Efficiency and Selectivity for Carbon Dioxide Electroreduction to Fuels on Tailored Copper Catalyst Architectures," *Energy Technol.*, vol. 4, no. 8, pp. 1020–1028, 2016.

[33] K. P. Kuhl, E. R. Cave, D. N. Abram, and T. F. Jaramillo, "New insights into the electrochemical reduction of carbon dioxide on metallic copper surfaces," *Energy Environ. Sci.*, vol. 5, no. 5, p. 7050, 2012.

[34] Q. Lu and F. Jiao, "Electrochemical CO2reduction: Electrocatalyst, reaction mechanism, and process engineering," *Nano Energy*, vol. 29, pp. 439–456, 2016.

[35] H. Ooka, M. C. Figueiredo, and M. T. M. Koper, "Competition between Hydrogen Evolution and Carbon Dioxide Reduction on Copper Electrodes in Mildly Acidic Media," *Langmuir*, vol. 33, no. 37, pp. 9307–9313, 2017.

[36] A. Y. Khodakov, W. Chu, and P. Fongarland, "Advances in the Development of Novel Cobalt Fischer − Tropsch Catalysts for Synthesis of Long-Chain Hydrocarbons and Clean Fuels Advances in the Development of Novel Cobalt Fischer − Tropsch Catalysts" *Am. Chem. Soc.*, vol. 107, no. 5, pp. 1692–1744, 2007.

[37] Y. Sekine, J. Filippi, M. Folliero, A. Lavacchi, H. A. Miller, A. Marchionni and F. Vizza, "An experimental study on Fischer-Tropsch catalysis: Implications for impact phenomena and nebular chemistry," *Meteorit. Planet. Sci.*, vol. 41, no. 5, pp. 715–729, May 2006.

[38] Y. Yao, D. Hildebrandt, D. Glasser, and X. Liu, "Fischer-tropsch synthesis using H2/CO/CO2 syngas mixtures over a cobalt catalyst," *Ind. Eng. Chem. Res.*, vol. 49, no. 21, pp. 11061–11066, 2010.

[39] L. P. Zhou, X. Hao, J. H. Gao, B. S. Wu, J. Xu, Y. Y. Xu and Y. W. Li, "Studies and discriminations of the kinetic models for the iron-based Fischer-Tropsch catalytic reaction in a recycle slurry reactor," *Energy and Fuels*, vol. 25, no. 1, pp. 52–59, 2011.

[40] F. G. Botes, J. W. Niemantsverdriet, and J. Van De Loosdrecht, "A comparison of cobalt and iron based slurry phase Fischer-Tropsch synthesis," *Catal. Today*, vol. 215, pp. 112–120, 2013.

[41] F. G. Botes, B. Van Dyk, and C. Mcgregor, "The Development of a Macro Kinetic Model for a Commercial Co / Pt / Al 2 O 3 Fischer - Tropsch Catalyst," vol. 2, no. 5, pp. 10439–10447, 2009.

[42] P. van Helden, J.-A. van den Berg, M. A. Petersen, W. Janse van Rensburg, I. M. Ciobîcă, and J. van de Loosdrecht, "Computational investigation of the kinetics and mechanism of the initial steps of the Fischer–Tropsch synthesis on cobalt," *Faraday Discuss.*, vol. 197, pp. 117–151, 2017.

[43] S. Mousavi, A. Zamaniyan, M. Irani, and M. Rashidzadeh, "Generalized kinetic model for iron and cobalt based Fischer-Tropsch synthesis catalysts: Review and model evaluation," *Appl. Catal. A Gen.*, vol. 506, pp. 57–66, 2015.

[44] H. J. Venvik and J. Yang, "Catalysis in microstructured reactors: Short review on small-scale syngas production and further conversion into methanol, DME and Fischer-Tropsch products," *Catal. Today*, vol. 285, pp. 135–146, 2017.

[45] F. G. Botes and B. B. Breman, "Development and testing of a new macro kinetic expression for the iron-based low-temperature Fischer-Tropsch reaction," *Ind. Eng. Chem. Res.*, vol. 45, no. 22, pp. 7415–7426, 2006.

[46] B. A. Rosen, A. Salehi-Khojin, M. R. Thorson, W. Zhu, D. T. Whipple, P. J. A. Kenis and R. I. Masel, "Ionic liquid-mediated selective conversion of CO2to CO at low overpotentials," *Science (80-.).*, vol. 334, no. 6056, pp. 643–644, 2011.

[47] S. Rönsch, J. Köchermann, J. Schneider, and S. Matthischke, "Global Reaction Kinetics of CO and CO2Methanation for Dynamic Process Modeling," *Chem. Eng. Technol.*, vol. 39, no. 2, pp. 208–218, 2016.

[48] "B50 Solar Cell," no. November. p. 3283, 2010.

[49] M. R. Singh, E. L. Clark, and A. T. Bell, "Thermodynamic and achievable efficiencies for solar-driven electrochemical reduction of carbon dioxide to transportation fuels," *Proc. Natl. Acad. Sci.*, vol. 112, no. 45, pp. E6111–E6118, 2015.

[50] G. Centi and S. Perathoner, "Opportunities and prospects in the chemical recycling of carbon dioxide to fuels," *Catal. Today*, vol. 148, no. 3–4, pp. 191–205, 2009.

[51] M. R. Singh, J. D. Goodpaster, A. Z. Weber, M. Head-Gordon, and A. T. Bell, "Mechanistic insights into electrochemical reduction of CO_2 over Ag using density functional theory and transport models," *Proc. Natl. Acad. Sci.*, p. 201713164, 2017.

[52] P. Olivier, C. Bourasseau, and B. Bouamama, "Modelling, simulation and analysis of a PEM electrolysis system," *IFAC-PapersOnLine*, vol. 49, no. 12, pp. 1014–1019, 2016.

[53] C. Graves, S. D. Ebbesen, M. Mogensen, and K. S. Lackner, "Sustainable hydrocarbon fuels by recycling CO2and H2O with renewable or nuclear energy," *Renew. Sustain. Energy Rev.*, vol. 15, no. 1, pp. 1–23, 2011.

[54] Y. D. Kim, C. Yang, B. KIm and J. H. Moon, "Corrigendum to 'Fischer–tropsch diesel production and evaluation as alternative automotive fuel in pilot-scale integrated biomass-to-liquid process' (Appl. Energy (2016) 180 (301–312) (S0306261916310364) (10.1016/j.apenergy.2016.07.095)) ," *Appl. Energy*, vol. 203, p. 982, 2017.

[55] "Heating systems Flow Rates," *The Engineering ToolBox*, 2004. [Online]. Available: http://www.engineeringtoolbox.com/carbon-monoxide-d_975.html. [Accessed: 01-Oct-2018].

[56] "Europe Average Daily Solar Hours (Solar Insolation)," 2010. [Online]. Available: http://www.hotspotenergy.com/DC-air-conditioner/europe-solar-hours.php.

[57] P. Ineichen, "Global irradiation: average and typical year, and year to year annual variability," *IEA Sol. Heat. Cool. Progr. Task 36*, no. september, p. 26, 2011.

[58] BP, "Statistical review of world energy 2018," 2018.

Annex I –Temperature Dependence of Rönsch's Model

In this section is presented the FTS rate temperature evolution for the nickel-based catalysts. As referred in 3.2-Fisher-Tropsch Synthesis, this model does not take in consideration the reverse reaction of methanation, being verified a steady growth of the FTS reaction rate in the region denoted in Figure A1, where there should be a decrease of the rate [47].

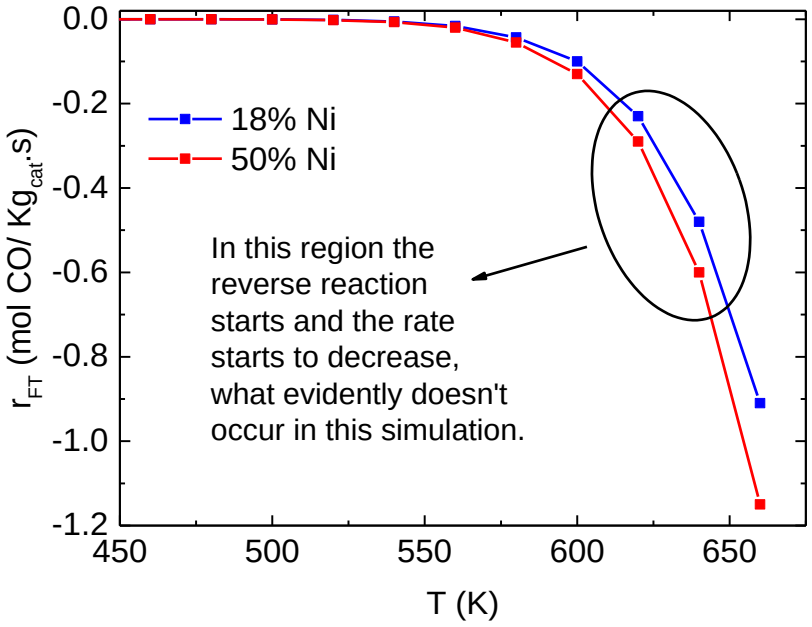

Figure A1 - Simulated FTS rates in function of temperature using Rönsch's kinetic model.

Annex II – Simulation Code for the Electrochemical Systems

In this section is provided the code used to simulate the electrochemical reactions.

```
(*CacheID: 234*)
(* Internal cache information:
NotebookFileLineBreakTest
NotebookFileLineBreakTest
NotebookDataPosition[       158,          7]
NotebookDataLength[     25907,        598]
NotebookOptionsPosition[     22921,        492]
NotebookOutlinePosition[     23586,        515]
CellTagsIndexPosition[     23543,        512]
WindowFrame->Normal*)

(* Beginning of Notebook Content *)
Notebook[{

Cell[CellGroupData[{
Cell["Electrochemical Simulation", "Title",
CellChangeTimes->{{3.7301006802322903`*^9,
3.7301007367072663`*^9}, {
3.747460380418911*^9, 3.747460396238901*^9}}],

Cell[CellGroupData[{

Cell["Parameters", "Section",
CellChangeTimes->{{3.7301007676757975`*^9,
3.7301007731763873`*^9}, {
3.747460399584248*^9, 3.7474604022883472`*^9}}],

Cell[CellGroupData[{

Cell[TextData[StyleBox["Activation voltages (V)",
"Subsection"]], "Subsection",
CellChangeTimes->{{3.7301024519332504`*^9,
3.730102477643181*^9}, {
3.730205826633988*^9, 3.7302058539529247`*^9},
{3.7474604069599037`*^9,
3.747460412300088*^9}}],

Cell["\<\
V0ch4 = 1.06;
V0co = 1.34; \
\>", "Input",
CellChangeTimes->{{3.730102464322665*^9,
3.730102483697239*^9}, {
3.7301025523213797`*^9, 3.730102570244741*^9},
{3.730102689180592*^9,
```

```
32    3.7301026898942423`*^9}, {3.730204391416199*^9,
      3.730204430399475*^9}, {
33    3.7302044683207664`*^9, 3.7302044886028404`*^9},
      {3.7302045283368034`*^9,
34    3.730204529695877*^9}, {3.7302048776023426`*^9,
      3.730204941623705*^9}, {
35    3.730456884462581*^9, 3.730456897260968*^9},
      {3.730459790698639*^9,
36    3.7304597975631385`*^9}, {3.730460254800928*^9,
      3.7304602597130313`*^9}, {
37    3.7304603414583488`*^9, 3.7304603458639984`*^9},
      {3.7305426245906477`*^9,
38    3.730542638405904*^9}, {3.730702280055341*^9,
      3.730702286176643*^9}, {
39    3.7324490859548435`*^9, 3.732449088288633*^9},
      {3.733204032512295*^9,
40    3.7332040356343937`*^9}, {3.747460417693777*^9,
      3.7474604271008096`*^9},
41    3.7474613803070283`*^9}]
42    }, Open  ]],

43    Cell[CellGroupData[{

44    Cell[TextData[StyleBox["Transfer coefficients ",
      "Subsection"]], "Subsection",
45    CellChangeTimes->{{3.730205392602815*^9,
      3.7302054649771743`*^9}, {
46    3.730205656086613*^9, 3.7302056646039443`*^9},
      {3.7302058775090632`*^9,
47    3.7302058987588997`*^9}, {3.7474604880067215`*^9,
      3.7474604968151493`*^9}}],

48    Cell[CellGroupData[{

49    Cell["CO", "Subsubsection",
50    CellChangeTimes->{{3.7302059265395956`*^9,
      3.7302059406781845`*^9}, {
51    3.732341790463298*^9, 3.7323418047461286`*^9},
      {3.747460508099435*^9,
52    3.7474605091773243`*^9}}],

53    Cell["\<\
54    \[Alpha]aco = 0;
55    \[Alpha]cco = 0.3; \
56    \>", "Input",
57    CellChangeTimes->{{3.730205959844035*^9,
      3.730205999791415*^9}, {
58    3.7317552612576175`*^9, 3.7317552630397153`*^9},
      {3.732341840064992*^9,
59    3.7323418502808695`*^9}, {3.732355334668562*^9,
      3.7323553589713736`*^9}, {
60    3.732355392732215*^9, 3.732355414318721*^9},
      {3.732355445928628*^9,
61    3.7323554506583166`*^9}, {3.7324514387011642`*^9,
62    3.7324514477053623`*^9}, {3.7324514920052524`*^9,
63    3.7324515182616444`*^9}, {3.732517807589095*^9,
      3.7325178091309853`*^9}, {
```

```
64    3.732517840138919*^9, 3.732517841205192*^9},
      {3.732518579719613*^9,
65    3.7325185822951*^9}, {3.732518751353256*^9,
      3.7325187517765665`*^9}, {
66    3.732526697765615*^9, 3.7325266985856533`*^9},
      {3.7329459865263605`*^9,
67    3.732945988495319*^9}, 3.732946137268297*^9,
      {3.7329464244203963`*^9,
68    3.732946426069195*^9}, {3.7329467345137463`*^9,
      3.7329467419206305`*^9}, {
69    3.7329468992362795`*^9, 3.7329468998459034`*^9},
      3.7329470431395245`*^9, {
70    3.733204048263543*^9, 3.7332040507707043`*^9},
      3.7474613803070283`*^9}]
71    }, Open  ]],

72    Cell[CellGroupData[{

73    Cell[TextData[StyleBox["CH4", "Subsection"]],
      "Subsubsection",
74    CellChangeTimes->{{3.732341824555127*^9,
      3.732341834116465*^9},
75    3.747460514100584*^9, {3.7483375926174235`*^9,
      3.748337605951787*^9}}],

76    Cell["\<\
77    \[Alpha]ach4 = 0;
78    \[Alpha]cch4 = 0.25; \
79    \>", "Input",
80    CellChangeTimes->{{3.732341862926966*^9,
      3.7323418692042217`*^9},
81    3.732345071183896*^9, {3.7323460974343853`*^9,
      3.7323461252645617`*^9}, {
82    3.7323461705941668`*^9, 3.732346171106098*^9},
      3.7325359241568365`*^9, {
83    3.733204056294365*^9, 3.733204061103676*^9},
      3.7474613803226147`*^9}]
84    }, Open  ]]
85    }, Open  ]],

86    Cell[CellGroupData[{

87    Cell["Exchange-current density (mA/cm^2)", "Subsection",
88    CellChangeTimes->{{3.7302062341657677`*^9,
      3.730206305977087*^9},
89    3.730206586399005*^9, {3.7474605187404785`*^9,
      3.7474605250105596`*^9}}],

90    Cell[CellGroupData[{

91    Cell["CO", "Subsubsection",
92    CellChangeTimes->{{3.730206625414463*^9,
      3.730206633945999*^9}, {
93    3.7304602201842513`*^9, 3.7304602206763077`*^9},
      {3.732344732151368*^9,
94    3.732344734389558*^9}, {3.747460353848879*^9,
      3.7474603539738426`*^9}}],
```

```
95    Cell["i0co = /10^3; ", "Input",
96    CellChangeTimes->{{3.7302066387968235`*^9,
      3.7302066516858535`*^9}, {
97    3.731755323047913*^9, 3.7317553233414726`*^9},
      {3.731755422694563*^9,
98    3.7317554230256624`*^9}, {3.73234476822007*^9,
      3.7323447698294706`*^9}, {
99    3.732451572100114*^9, 3.732451611662155*^9},
      {3.732451829264825*^9,
100   3.732451835802194*^9}, {3.732451882687908*^9,
      3.7324518924670706`*^9}, {
101   3.7325165814117556`*^9, 3.732516581812768*^9},
      3.7325168868717146`*^9, {
102   3.7325171799113517`*^9, 3.732517180552961*^9},
      {3.7325176172668486`*^9,
103   3.7325176176189475`*^9}, {3.73251778708307*^9,
      3.7325177908416305`*^9}, {
104   3.73251817169418*^9, 3.7325181744516954`*^9},
      {3.732518311964279*^9,
105   3.7325183163697844`*^9}, {3.7325185724402924`*^9,
      3.732518572832698*^9}, {
106   3.7325343513552933`*^9, 3.732534351834137*^9},
      3.7332040687623973`*^9,
107   3.7474613803226147`*^9, {3.7483257441647124`*^9,
      3.748325754696561*^9}}]
108   }, Open  ]],

109   Cell[CellGroupData[{

110   Cell["CH4", "Subsubsection",
111   CellChangeTimes->{{3.7323447395525866`*^9,
      3.7323447465910316`*^9}, {
112   3.7474603568355117`*^9, 3.74746036082487*^9}}],

113   Cell["i0ch4 = 1.5/10^3; ", "Input",
114   CellChangeTimes->{{3.732344751265006*^9,
      3.7323447635644617`*^9}, {
115   3.732344843158413*^9, 3.732344844065092*^9},
      {3.7323449978552437`*^9,
116   3.732345038409955*^9}, 3.733204072916088*^9,
      3.74746138033825*^9}]
117   }, Open  ]]
118   }, Open  ]],

119   Cell[CellGroupData[{

120   Cell["Overpotential", "Subsection",
121   CellChangeTimes->{{3.731750696611108*^9,
      3.7317507092911844`*^9}}],

122   Cell["\<\
123   opco2 = 0.67;
124   opch4 = 0.9; \
125   \>", "Input",
126   CellChangeTimes->{{3.7317507279732895`*^9,
      3.7317507557330685`*^9}, {
127   3.731751014767687*^9, 3.731751021093195*^9},
      {3.731754126559633*^9,
```

```
128   3.73175412689065*^9}, {3.732343088781472*^9,
      3.7323430892867107`*^9}, {
129   3.7323443374149084`*^9, 3.73234433789172*^9},
      {3.7323453382017746`*^9,
130   3.732345338689353*^9}, {3.732352695960335*^9,
      3.7323526961472087`*^9}, {
131   3.7323534839820004`*^9, 3.732353490884509*^9},
      {3.732354532711167*^9,
132   3.7323545331438556`*^9}, {3.7323553058174434`*^9,
      3.732355324224152*^9}, {
133   3.732355456905587*^9, 3.7323554574944158`*^9},
      {3.7323609198554726`*^9,
134   3.7323609201550393`*^9}, {3.73236100080093*^9,
      3.732361001289295*^9}, {
135   3.7324471522226925`*^9, 3.732447157313941*^9},
      {3.732447221212305*^9,
136   3.7324472216802635`*^9}, {3.732447293035773*^9,
      3.7324472934150076`*^9}, {
137   3.7324475139122515`*^9, 3.732447514249719*^9},
      {3.7324477231964912`*^9,
138   3.732447732451832*^9}, {3.7324480038837447`*^9,
      3.732448004641085*^9}, {
139   3.732448195031867*^9, 3.732448195504206*^9},
      3.7324490781431255`*^9, {
140   3.7324514106095533`*^9, 3.732451411255643*^9},
      {3.732517358415578*^9,
141   3.732517358922106*^9}, 3.732517800169287*^9,
      {3.732517978193007*^9,
142   3.732517978663689*^9}, {3.7325181837779207`*^9,
      3.7325181845856695`*^9}, {
143   3.7325344912481375`*^9, 3.7325344922203903`*^9},
      {3.7325346052856936`*^9,
144   3.7325346071318507`*^9}, {3.732535437583633*^9,
      3.732535438041718*^9}, {
145   3.732535686193164*^9, 3.7325356874266214`*^9},
      {3.7325361008154483`*^9,
146   3.7325361012497196`*^9}, {3.7325366623104877`*^9,
      3.732536663291227*^9}, {
147   3.7325367997555313`*^9, 3.732536800667230 6`*^9},
      {3.7325370948848944`*^9,
148   3.732537095701105*^9}, {3.7325372133405333`*^9,
      3.7325372139507327`*^9},
149   3.732537340403219*^9, {3.732945810223598*^9,
      3.732945811880104*^9}, {
150   3.7329468921731844`*^9, 3.732946892657611*^9},
      {3.7332040764152317`*^9,
151   3.7332040832575893`*^9}, {3.7474603269274263`*^9,
      3.7474603290362396`*^9},
152   3.74746138033825*^9}]
153   }, Open  ]],

154   Cell[CellGroupData[{

155   Cell["Constants", "Subsection",
156   CellChangeTimes->{{3.7301121138593903`*^9,
      3.730112125374169*^9},
157   3.7474605288975306`*^9}],
```

```
158   Cell["\<\
159   T = 310;
160   F = 96487;
161   R = 8.314;
162   Adv = 6.022*10^23;
163   Vm = 22.414; \
164   \>", "Input",
165   CellChangeTimes->{{3.7301121295150576`*^9,
      3.7301121306716022`*^9}, {
166   3.730120251424306*^9, 3.73012028695747*^9},
      {3.73012034114322*^9,
167   3.730120376597106*^9}, {3.7301216658836756`*^9,
      3.7301216991397595`*^9}, {
168   3.7301218088915744`*^9, 3.7301218223825903`*^9},
      {3.73019938844477*^9,
169   3.7301997467532697`*^9}, 3.7301997778503485`*^9,
      {3.7302042920709887`*^9,
170   3.7302043037739396`*^9}, {3.730204352885289*^9,
      3.7302043813837786`*^9}, {
171   3.732346188107482*^9, 3.7323461888222637`*^9},
      {3.7323462248096857`*^9,
172   3.732346225628833*^9}, {3.7324516298003006`*^9,
      3.7324516301295557`*^9}, {
173   3.7325365100929856`*^9, 3.732536510358493*^9},
      {3.7331368125256042`*^9,
174   3.7331368313113356`*^9}, {3.733204088136694*^9,
      3.733204095529003*^9}, {
175   3.7346943851419168`*^9, 3.7346943997116623`*^9},
      3.7474613803538604`*^9, {
176   3.7476328219542923`*^9, 3.747632823486209*^9},
      {3.747634846935521*^9,
177   3.747634847322158*^9}, {3.7476377000191154`*^9,
      3.7476377013780966`*^9}, {
178   3.7476463304362097`*^9, 3.747646332090849*^9},
      {3.7476468353106413`*^9,
179   3.7476468358837795`*^9}, {3.7476471679526353`*^9,
180   3.7476471684271355`*^9}, {3.7476474401462917`*^9,
      3.747647444110482*^9}}]
181   }, Open  ]]
182   }, Open  ]],

183   Cell[CellGroupData[{

184   Cell["Model", "Section",
185   CellChangeTimes->{{3.730205002790074*^9,
      3.7302050070554333`*^9}, {
186   3.747460531849174*^9, 3.747460532911398*^9}}],

187   Cell[CellGroupData[{

188   Cell["CO", "Subsection",
189   CellChangeTimes->{{3.7302050188095407`*^9,
      3.7302050256496677`*^9}, {
190   3.7474605366626387`*^9, 3.7474605369126034`*^9}}],

191   Cell["\<\
192   ico[v_] = i0co*(E^((\[Alpha]aco*F*(v - opco2 -
      V0co))/(R*T)) - \
```

```
193   E^((\[Alpha]cco*F*(v - opco2 - V0co))/(R*T))); \
194   \>", "Input",
195   CellChangeTimes->{{3.730205062274109*^9,
      3.7302052080241103`*^9}, {
196   3.730205273195899*^9, 3.730205369258644*^9},
      {3.7302060159085236`*^9,
197   3.7302060366181383`*^9}, {3.730206663899069*^9,
      3.730206683086957*^9}, {
198   3.7304569154190054`*^9, 3.730456926432851*^9},
      {3.7304570278572044`*^9,
199   3.730457040139948*^9}, {3.7307159574189153`*^9,
      3.7307159641496277`*^9}, {
200   3.7317509434021254`*^9, 3.7317509528786235`*^9},
      {3.731751050243702*^9,
201   3.7317510665837507`*^9}, {3.731751099463339*^9,
      3.7317511271199303`*^9}, {
202   3.7323418861556273`*^9, 3.7323418898592353`*^9},
      {3.732344859536743*^9,
203   3.7323448607907815`*^9}, {3.7474604335429554`*^9,
      3.747460444662143*^9},
204   3.7474613803850994`*^9}]
205   }, Open  ]],

206   Cell[CellGroupData[{

207   Cell["CH4", "Subsection",
208   CellChangeTimes->{{3.7302060586806355`*^9,
      3.7302060641645036`*^9}, {
209   3.7474605392558575`*^9, 3.747460539552535*^9}}],

210   Cell["\<\
211   ich4[v_] = i0ch4*(E^((\[Alpha]ach4*F*(v - opch4 -
      V0ch4))/(R*T)) - E^((\
212   \[Alpha]cch4*F*(v - opch4 - V0ch4))/(R*T))); \
213   \>", "Input",
214   CellChangeTimes->{{3.7302060764463406`*^9,
      3.7302060886806436`*^9}, {
215   3.7302066743120594`*^9, 3.730206677508562*^9},
      {3.7302067171814756`*^9,
216   3.7302067189925704`*^9}, {3.7304569288862348`*^9,
217   3.7304569459036956`*^9}, {3.7304570295138025`*^9,
      3.730457046656121*^9}, {
218   3.7307042971974936`*^9, 3.730704307704194*^9},
      {3.7307043835390577`*^9,
219   3.7307044096611195`*^9}, {3.7307158259575787`*^9,
      3.730715836444783*^9}, {
220   3.73071590841877*^9, 3.7307159131704807`*^9},
      {3.7317507865192027`*^9,
221   3.73175079096616*^9}, {3.731750870820841*^9,
      3.7317508796142855`*^9}, {
222   3.731750936549057*^9, 3.731750940863552*^9},
      {3.7317554924609623`*^9,
223   3.7317555381622844`*^9}, {3.732341895620638*^9,
      3.7323419022627773`*^9}, {
224   3.7323448536709776`*^9, 3.73234489450574*^9},
      {3.732344927417533*^9,
225   3.732344948391952*^9}, {3.732344982593966*^9,
      3.7323450105379925`*^9}, {
```

```
226   3.747460448208477*^9, 3.7474604525830326`*^9},
      3.7474613804154305`*^9}]
227   }, Open  ]]
228   }, Open  ]],

229   Cell[CellGroupData[{

230   Cell["Curves JvsV (mA/cm^2 vs V)", "Section",
231   CellChangeTimes->{{3.7302067329931307`*^9,
      3.7302067372116823`*^9}, {
232   3.7304579684338665`*^9, 3.7304580068269444`*^9},
      {3.747460543084216*^9,
233   3.747460552026987*^9}}],

234   Cell[CellGroupData[{

235   Cell["CO", "Subsection",
236   CellChangeTimes->{{3.7302067506926575`*^9,
      3.7302067551023064`*^9}}],

237   Cell["JVco = Plot[ico[v], {v, 0, 3.3}];", "Input",
238   CellChangeTimes->{{3.7281287725833864`*^9,
      3.72812878499098*^9}, {
239   3.728128816463109*^9, 3.7281288582957134`*^9},
      {3.728128960958708*^9,
240   3.728128977148052*^9}, {3.728129135758653*^9,
      3.7281291362430563`*^9}, {
241   3.728129778050099*^9, 3.728129786021245*^9},
      {3.728130897796398*^9,
242   3.728130902765664*^9}, {3.72813098290084*^9,
      3.728130989464047*^9}, {
243   3.7281318819322896`*^9, 3.728131918452166`*^9},
      {3.7282125639610715`*^9,
244   3.7282126370875483`*^9}, {3.728212797490885*^9,
      3.728212802821065*^9},
245   3.728218011243063*^9, {3.728297986170039*^9,
      3.7282979913738947`*^9}, {
246   3.7283000777692256`*^9, 3.728300110688217*^9},
      {3.7283007429181747`*^9,
247   3.728300743319805*^9}, {3.728300962448844*^9,
      3.7283009628633146`*^9}, {
248   3.7283018232416673`*^9, 3.7283018325603266`*^9},
      {3.7302067722901464`*^9,
249   3.7302067795395455`*^9}, {3.7304569820710535`*^9,
250   3.7304570145278425`*^9}, {3.730457067674139*^9,
      3.73045707815965*^9}, {
251   3.7304598165057993`*^9, 3.7304598175822735`*^9},
      {3.730459871343205*^9,
252   3.7304598724611397`*^9}, {3.730460232965739*^9,
      3.73046023848231*^9}, {
253   3.7304602713463697`*^9, 3.7304602820202675`*^9},
      {3.730460316958253*^9,
254   3.7304603183094006`*^9}, {3.7305426660669127`*^9,
255   3.7305426858674335`*^9}, {3.730548271159131*^9,
      3.7305482751091423`*^9}, {
256   3.7307022986418977`*^9, 3.7307023221938915`*^9},
      {3.730715975539633*^9,
```

```
257   3.730715987647316*^9}, {3.7323524112009974`*^9,
      3.7323524240972776`*^9}, {
258   3.7323527046257105`*^9, 3.7323527352448106`*^9},
      {3.732353525415127*^9,
259   3.732353570178111*^9}, {3.732354559542489*^9,
      3.732354569566208*^9}, {
260   3.7323549941952934`*^9, 3.732354995122881*^9},
      {3.732355370195488*^9,
261   3.732355379944004*^9}, {3.732355425288506*^9,
      3.7323554359713917`*^9}, {
262   3.732355472557393*^9, 3.732355490945881*^9},
      {3.7324514635672803`*^9,
263   3.732451536002836*^9}, {3.7324516425488253`*^9,
      3.7324516603406086`*^9}, {
264   3.732517198192904*^9, 3.732517198489897*^9},
      {3.732517855756573*^9,
265   3.7325178567567883`*^9}, {3.732517990021613*^9,
      3.732518001351486*^9}, {
266   3.732518326992695*^9, 3.732518328017044*^9},
      {3.7325187629634686`*^9,
267   3.7325188053457775`*^9}, {3.7329458352745485`*^9,
268   3.7329458359933977`*^9}, {3.732946753593871*^9,
      3.7329467539844046`*^9}, {
269   3.732947055953224*^9, 3.7329470567972145`*^9},
      3.7474602030681467`*^9,
270   3.747461380444225*^9, {3.747632845179334*^9,
      3.7476328455302672`*^9},
271   3.7483374612772408`*^9}],

272   Cell["Export[\"JVco.txt\", JVco];", "Input",
273   CellChangeTimes->{{3.7305483195326033`*^9,
      3.730548390458208*^9}, {
274   3.730549167816127*^9, 3.730549190602865*^9},
      3.7325355017111993`*^9,
275   3.7325371185543985`*^9, 3.747461380444225*^9,
      {3.7483374930772376`*^9,
276   3.7483374997613716`*^9}}],

277   Cell["SystemOpen[\"JVco.txt\"];", "Input",
278   CellChangeTimes->{3.7474613804754677`*^9,
      3.748337490897064*^9},
279   NumberMarks->False]
280   }, Open  ]],

281   Cell[CellGroupData[{

282   Cell["CH4", "Subsection",
283   CellChangeTimes->{{3.7305482605210724`*^9,
      3.7305482652110786`*^9}}],

284   Cell["JVch4 = Plot[ich4[v], {v, 0, 3.6}];", "Input",
285   CellChangeTimes->{{3.730457114064476*^9,
      3.73045711511164*^9}, {
286   3.73045982173118*^9, 3.730459822847386*^9},
      {3.730459860257827*^9,
287   3.7304598654356413`*^9}, {3.730460325468667*^9,
      3.730460326477806*^9}, {
```

```
288   3.7305426898891697`*^9, 3.7305427149855137`*^9},
      {3.7305435663568783`*^9,
289   3.730543573442979*^9}, {3.730551647056983*^9,
      3.7305516838801785`*^9}, {
290   3.7307023105460777`*^9, 3.730702329241274*^9},
      {3.730715851231162*^9,
291   3.7307158861604757`*^9}, {3.730715922139833*^9,
      3.730715945533636*^9}, {
292   3.7317508075998683`*^9, 3.731750808826939*^9},
      {3.7317511534774 56*^9,
293   3.7317511702090683`*^9}, {3.7317541431566954`*^9,
      3.7317541479414287`*^9},
294   3.731755367748865*^9, {3.731755456286014*^9,
      3.7317554708862934`*^9}, {
295   3.732343113776225*^9, 3.7323431313250723`*^9},
      {3.7323443497600756`*^9,
296   3.732344369550 76*^9}, {3.7323452904962854`*^9,
      3.732345297099603*^9}, {
297   3.732345350638051*^9, 3.732345370197008*^9},
      {3.7323461485163417`*^9,
298   3.732346164123357*^9}, {3.7323462395817566`*^9,
      3.732346241234708*^9}, {
299   3.732535268013749*^9, 3.732535274718278*^9},
      {3.7325356986279087`*^9,
300   3.7325356995025206`*^9}, {3.7325359423453083`*^9,
301   3.7325359484170523`*^9}, {3.7325361110158014`*^9,
      3.7325361116178837`*^9},
302   3.7474602059907007`*^9, 3.7474613804910874`*^9,
      {3.7476328498276014`*^9,
303   3.7476328504392633`*^9}, 3.748337464279213*^9}],

304   Cell["Export[\"JVch4.txt\", JVch4];", "Input",
305   CellChangeTimes->{{3.730551527715 96*^9,
      3.7305515662728214`*^9}, {
306   3.732536681159367*^9, 3.732536685016992*^9},
      3.7474613804910874`*^9,
307   3.7483374956214705`*^9}],

308   Cell["SystemOpen[\"JVch4.txt\"];", "Input",
309   CellChangeTimes->{3.74746138050671*^9,
      3.748337484401429*^9},
310   NumberMarks->False]
311   }, Open  ]]
312   }, Open  ]],

313   Cell[CellGroupData[{

314   Cell["Efficiencies", "Section",
315   CellChangeTimes->{{3.7307201624182577`*^9,
      3.7307201828657002`*^9}, {
316   3.747460558693102*^9, 3.7474605619284964`*^9}}],

317   Cell[CellGroupData[{

318   Cell["E.E.", "Subsection",
319   CellChangeTimes->{{3.730720190983801*^9,
      3.730720193381843*^9}, {
320   3.732949379836095*^9, 3.732949380586351*^9}}],
```

```
321   Cell["\<\
322   eeco = (E0co/(E0co + opco2))*efco;
323   eech4 = (E0ch4/(E0ch4 + opch4))*efch4;
324   eeh2 = (E0h2o/(E0h2o + oph2))*efh2;
325   efco = 1;
326   efch4 = 0.8;
327   efh2 = 1; \
328   \>", "Input",
329   CellChangeTimes->{{3.732949387680731*^9,
      3.7329496023689365`*^9}, {
330   3.7346718278029013`*^9, 3.7346718719205437`*^9},
      {3.734672103678*^9,
331   3.734672124222434*^9}, {3.7347767398768487`*^9,
      3.734776742752269*^9}, {
332   3.734776783898782*^9, 3.734776803402712*^9},
      {3.735626917945689*^9,
333   3.7356269184433746`*^9}, {3.735627025766329*^9,
      3.73562704276167*^9}, {
334   3.7371084061823635`*^9, 3.7371084087919865`*^9},
      {3.7371085525831327`*^9,
335   3.737108553974264*^9}, {3.740725622916138*^9,
      3.740725623457694*^9}, {
336   3.7407256666173196`*^9, 3.7407256872351923`*^9},
      {3.742037242517683*^9,
337   3.7420372491831193`*^9}, {3.7473966919084554`*^9,
338   3.7473966947354517`*^9}, {3.7474602132077665`*^9,
339   3.7474602184282713`*^9}, {3.7474604633813696`*^9,
      3.747460467458949*^9},
340   3.7474613805223336`*^9}]
341   }, Open  ]]
342   }, Open  ]],

343   Cell[CellGroupData[{

344   Cell["Production", "Section",
345   CellChangeTimes->{{3.7331361968741913`*^9,
      3.7331361998931684`*^9}, {
346   3.733136262017668*^9, 3.7331362781648865`*^9},
      {3.7474605735696135`*^9,
347   3.747460576631632*^9}}],

348   Cell[CellGroupData[{

349   Cell["CH4", "Subsection",
350   CellChangeTimes->{{3.733136285105114*^9,
      3.7331362861346254`*^9}}],

351   Cell["\<\
352   Iintch4 = 5.69;
353   t = 3600;
354   nch4 = 8; \
355   \>", "Input",
356   CellChangeTimes->{{3.733136343477504*^9,
      3.7331363739676943`*^9}, {
357   3.7331364150683613`*^9, 3.733136420516441*^9},
      {3.73313672209429*^9,
```

```
358   3.733136722780589*^9}, {3.7331375467062693`*^9,
      3.733137554281413*^9}, {
359   3.7332041715552177`*^9, 3.7332041871686296`*^9},
      {3.734671719992342*^9,
360   3.734671720557977*^9}, {3.734671766837264*^9,
      3.734671770874631*^9}, {
361   3.734937063924534*^9, 3.7349370891218863`*^9},
      {3.742022205296294*^9,
362   3.7420222326199555`*^9}, {3.7420341951799545`*^9,
363   3.7420342174918733`*^9}, {3.742037494158535*^9,
      3.742037495137986*^9}, {
364   3.7420378083704724`*^9, 3.7420378103288846`*^9},
      {3.7421193392727566`*^9,
365   3.742119355838048*^9}, {3.7421194177457724`*^9,
      3.742119423332254*^9}, {
366   3.7458358268514247`*^9, 3.745835833646872*^9},
      3.747461380537973*^9}],

367   Cell["\<\
368   nfch4 = ((Iintch4*t)/(nch4*F))*eech4;
369   Vch4 = nfch4*Vm; \
370   \>", "Input",
371   CellChangeTimes->{{3.7331363865465674`*^9,
      3.7331364856109533`*^9}, {
372   3.7331368578905325`*^9, 3.7331368819407835`*^9},
      {3.733137539017995*^9,
373   3.7331375421005516`*^9}, {3.7346717969950805`*^9,
      3.734671797681855*^9}, {
374   3.734694410397667*^9, 3.73469443606054*^9},
      {3.7346944904843645`*^9,
375   3.734694495180335*^9}, {3.7349370915587883`*^9,
      3.7349371335062723`*^9}, {
376   3.7349371660921526`*^9, 3.734937171688223*^9},
      {3.7356267736374226`*^9,
377   3.7356267759209704`*^9}, {3.737110042489417*^9,
      3.737110042710823*^9}, {
378   3.737110173450137*^9, 3.737110174715786*^9},
      {3.7371102413794537`*^9,
379   3.737110290006397*^9}, {3.7474602228196273`*^9,
      3.7474602321939025`*^9}, {
380   3.7474602804458857`*^9, 3.747460281577194*^9},
      3.747461380537973*^9}]
381   }, Open  ]],

382   Cell[CellGroupData[{

383   Cell["Syngas", "Subsection",
384   CellChangeTimes->{{3.733136946828434*^9,
      3.7331369533358264`*^9}}],

385   Cell["\<\
386   Iint = {5.74, 11.5, 17.25, 23.18, 28, 33.38, 38.86, 44.12,
      49.48, 55, 85.7, \
387   113.6, 141.5, 169, 224.2,
388   279.5};
389   t = 3600;
390   n = 2; \
391   \>", "Input",
```

```
392   CellChangeTimes->{{3.7331368514849577`*^9,
      3.7331368532025657`*^9}, {
393   3.733136967912961*^9, 3.7331370037958174`*^9},
      {3.7331374283766594`*^9,
394   3.733137450899485*^9}, {3.7332041926912374`*^9,
      3.73320420736794*^9}, {
395   3.7346717231828957`*^9, 3.734671723908554*^9},
      {3.7346717638072343`*^9,
396   3.734671764735155*^9}, {3.734694799163391*^9,
      3.734694800494834*^9}, {
397   3.7420221306493 36*^9, 3.7420221732140207`*^9},
      {3.7420343108534956`*^9,
398   3.742034339773822*^9}, {3.74203746025386*^9,
      3.7420374612828484`*^9}, {
399   3.7420378420126033`*^9, 3.7420378464140425`*^9},
      3.742119672231184*^9, {
400   3.7421200663958282`*^9, 3.7421200801350965`*^9},
      {3.7421201772120657`*^9,
401   3.74212018380202*^9}, {3.7458358010139256`*^9,
      3.7458358155105004`*^9}, {
402   3.7459048492054715`*^9, 3.745904916913404*^9},
      {3.7459050657882185`*^9,
403   3.7459050872538147`*^9}, {3.74739734061827*^9,
      3.7473974166154027`*^9},
404   3.7474613805535746`*^9}],

405   Cell["\<\
406   nco = ((Iint*t)/(n*F))*eeco;
407   nh2 = ((Iint*t)/(n*F))*eeh2;
408   Vco = nco*Vm;
409   Vh2 = nh2*Vm; \
410   \>", "Input",
411   CellChangeTimes->{{3.7331369954272947`*^9,
      3.733137054066056*^9}, {
412   3.733137397580514*^9, 3.7331374232809796`*^9},
      {3.7332042436226597`*^9,
413   3.733204291706519*^9}, {3.7346717816543283`*^9,
      3.734671792697092*^9}, {
414   3.734672981177861*^9, 3.73467298689581*^9},
      {3.7346948092435884`*^9,
415   3.7346948267182817`*^9}, 3.737112622756745*^9,
      {3.737112660915682*^9,
416   3.7371127616961365`*^9}, {3.7371129125736003`*^9,
      3.737112914103511*^9}, {
417   3.747460237271042*^9, 3.7474602424735436`*^9},
      3.7474613805691943`*^9}]
418   }, Open  ]]
419   }, Open  ]]
420   }, Open  ]]
421   },
422   WindowSize->{1902, 976},
423   WindowMargins->{{-9, Automatic}, {Automatic, 0}},
424   PrintingCopies->1,
425   PrintingPageRange->{32000, 32000},
426   PrintingOptions->{"Magnification"->1.,
427   "PaperOrientation"->"Portrait",
428   "PaperSize"->{595.3199999999999, 841.9200000000001}},
429   TaggingRules->{"$testsRun" -> False},
```

```
430   Magnification:>1.5 Inherited,
431   FrontEndVersion->"11.0 for Microsoft Windows (64-bit)
      (September 21, 2016)",
432   StyleDefinitions->FrontEnd`FileName[{"Report"},
      "StandardReport.nb",
433   CharacterEncoding -> "UTF-8"]
434   ]
435   (* End of Notebook Content *)

436   (* Internal cache information *)
437   (*CellTagsOutline
438   CellTagsIndex->{}
439   *)
440   (*CellTagsIndex
441   CellTagsIndex->{}
442   *)
443   (*NotebookFileOutline
444   Notebook[{
445   Cell[CellGroupData[{
446   Cell[580, 22, 162, 2, 147, "Title"],
447   Cell[CellGroupData[{
448   Cell[767, 28, 150, 2, 109, "Section"],
449   Cell[CellGroupData[{
450   Cell[942, 34, 249, 3, 54, "Subsection"],
451   Cell[1194, 39, 905, 15, 84, "Input"]
452   }, Open  ]],
453   Cell[CellGroupData[{
454   Cell[2136, 59, 300, 3, 54, "Subsection"],
455   Cell[CellGroupData[{
456   Cell[2461, 66, 199, 3, 52, "Subsubsection"],
457   Cell[2663, 71, 1068, 17, 84, "Input"]
458   }, Open  ]],
459   Cell[CellGroupData[{
460   Cell[3768, 93, 202, 2, 54, "Subsubsection"],
461   Cell[3973, 97, 359, 7, 84, "Input"]
462   }, Open  ]]
463   }, Open  ]],
464   Cell[CellGroupData[{
465   Cell[4381, 110, 200, 2, 54, "Subsection"],
466   Cell[CellGroupData[{
467   Cell[4606, 116, 243, 3, 52, "Subsubsection"],
468   Cell[4852, 121, 932, 12, 59, "Input"]
469   }, Open  ]],
470   Cell[CellGroupData[{
471   Cell[5821, 138, 148, 2, 52, "Subsubsection"],
472   Cell[5972, 142, 248, 3, 59, "Input"]
473   }, Open  ]]
474   }, Open  ]],
475   Cell[CellGroupData[{
476   Cell[6269, 151, 103, 1, 54, "Subsection"],
477   Cell[6375, 154, 2043, 30, 84, "Input"]
478   }, Open  ]],
479   Cell[CellGroupData[{
480   Cell[8455, 189, 127, 2, 54, "Subsection"],
481   Cell[8585, 193, 1285, 22, 157, "Input"]
482   }, Open  ]]
483   }, Open  ]],
484   Cell[CellGroupData[{
```

```
485   Cell[9919, 221, 141, 2, 109, "Section"],
486   Cell[CellGroupData[{
487   Cell[10085, 227, 147, 2, 54, "Subsection"],
488   Cell[10235, 231, 845, 13, 59, "Input"]
489   }, Open  ]],
490   Cell[CellGroupData[{
491   Cell[11117, 249, 146, 2, 54, "Subsection"],
492   Cell[11266, 253, 1102, 16, 59, "Input"]
493   }, Open  ]]
494   }, Open  ]],
495   Cell[CellGroupData[{
496   Cell[12417, 275, 217, 3, 109, "Section"],
497   Cell[CellGroupData[{
498   Cell[12659, 282, 94, 1, 54, "Subsection"],
499   Cell[12756, 285, 2496, 34, 59, "Input"],
500   Cell[15255, 321, 290, 4, 59, "Input"],
501   Cell[15548, 327, 129, 2, 92, "Input"]
502   }, Open  ]],
503   Cell[CellGroupData[{
504   Cell[15714, 334, 95, 1, 54, "Subsection"],
505   Cell[15812, 337, 1433, 19, 59, "Input"],
506   Cell[17248, 358, 215, 3, 59, "Input"],
507   Cell[17466, 363, 127, 2, 59, "Input"]
508   }, Open  ]]
509   }, Open  ]],
510   Cell[CellGroupData[{
511   Cell[17642, 371, 152, 2, 109, "Section"],
512   Cell[CellGroupData[{
513   Cell[17819, 377, 141, 2, 54, "Subsection"],
514   Cell[17963, 381, 979, 19, 168, "Input"]
515   }, Open  ]]
516   }, Open  ]],
517   Cell[CellGroupData[{
518   Cell[18991, 406, 201, 3, 106, "Section"],
519   Cell[CellGroupData[{
520   Cell[19217, 413, 93, 1, 72, "Subsection"],
521   Cell[19313, 416, 862, 15, 94, "Input"],
522   Cell[20178, 433, 834, 13, 70, "Input"]
523   }, Open  ]],
524   Cell[CellGroupData[{
525   Cell[21049, 451, 96, 1, 72, "Subsection"],
526   Cell[21148, 454, 1095, 19, 119, "Input"],
527   Cell[22246, 475, 635, 12, 119, "Input"]
528   }, Open  ]]
529   }, Open  ]]
530   }, Open  ]]
531   }
532   ]
533   *)
```

Annex III – Simulation Code for the Fischer-Tropsch Synthesis

Here is presented the code used to simulate the reaction rate of the FTS process.

```
(*CacheID: 234*)
(* Internal cache information:
NotebookFileLineBreakTest
NotebookFileLineBreakTest
NotebookDataPosition[       158,          7]
NotebookDataLength[      9906,        316]
NotebookOptionsPosition[      8520,        264]
NotebookOutlinePosition[      9024,        282]
CellTagsIndexPosition[      8981,        279]
WindowFrame->Normal*)

(* Beginning of Notebook Content *)
Notebook[{

Cell[CellGroupData[{
Cell["Fischer-Tropsch Synthesis", "Title",
CellChangeTimes->{{3.7334706022698045`*^9,
3.733470632452544*^9}}],

Cell[CellGroupData[{

Cell["Parameters", "Section",
CellChangeTimes->{{3.733470693756769*^9,
3.7334707004833455`*^9}, {
3.7335539402987385`*^9, 3.7335539416003613`*^9},
{3.74746229836588*^9,
3.747462300719948*^9}}],

Cell[CellGroupData[{

Cell["Constants", "Subsection",
CellChangeTimes->{{3.7346806452941093`*^9,
3.734680648468276*^9},
3.747462303674736*^9}],

Cell[BoxData[{
RowBox[{
RowBox[{"A", "=",
RowBox[{"10", "^",
RowBox[{"-", "3"}]}]}], ";"}], "\[IndentingNewLine]",
RowBox[{
RowBox[{"K1co", "=", "0.428"}], ";"}],
"\[IndentingNewLine]",
RowBox[{
RowBox[{"K2co", "=", "0.165"}], ";"}],
"\[IndentingNewLine]",
RowBox[{
RowBox[{"Pco", "=",
```

```
36    RowBox[{"Range", "[",
37    RowBox[{"0", ",", "20", ",", "1"}], "]"}]}], ";"}],
      "\[IndentingNewLine]",
38    RowBox[{
39    RowBox[{"Ph2", "=",
40    RowBox[{"3", "*", "Pco"}]}], ";"}], "\[IndentingNewLine]",
41    RowBox[{
42    RowBox[{"k0klose", "=",
43    RowBox[{"4.2", "*",
44    RowBox[{"10", "^", "9"}]}]}], ";"}],
      "\[IndentingNewLine]",
45    RowBox[{
46    RowBox[{"k0zhang", "=",
47    RowBox[{"5.3", "*",
48    RowBox[{"10", "^", "9"}]}]}], ";"}],
      "\[IndentingNewLine]",
49    RowBox[{
50    RowBox[{"Tg", "=", "533"}], ";"}], "\[IndentingNewLine]",
51    RowBox[{
52    RowBox[{"E1", "=", "103000"}], ";"}],
      "\[IndentingNewLine]",
53    RowBox[{
54    RowBox[{"R", "=", "8.314"}], ";"}], "\[IndentingNewLine]",
55    RowBox[{
56    RowBox[{"\[CapitalDelta]Hh", "=",
57    RowBox[{"-", "16000"}]}], ";"}], "\[IndentingNewLine]",
58    RowBox[{
59    RowBox[{"\[CapitalDelta]Hc", "=",
60    RowBox[{"-", "42000"}]}], ";"}], "\[IndentingNewLine]",
61    RowBox[{
62    RowBox[{"K0c", "=",
63    RowBox[{"5.8", "*",
64    RowBox[{"10", "^",
65    RowBox[{"-", "4"}]}]}]}], ";"}], "\[IndentingNewLine]",
66    RowBox[{
67    RowBox[{"K0h", "=",
68    RowBox[{"1.6", "*",
69    RowBox[{"10", "^",
70    RowBox[{"-", "2"}]}]}]}], ";"}]}], "Input",
71    CellChangeTimes->CompressedData["
72    1:eJwd0FsogwEYxvHPzMqa7IYkc4ilnKYkDGWGJC0toaSWWaFYlBpzilJz
      Q05r
73    5Tgl1saFSS2Fm0kOWZtoVy7mQl9hzlYO3/NePP16bv8prXq1jscwTBI3WP
      Wl
74    1+Z6WIXVJ++EKmvXMaw4nzyBOuH7QIOXVTyZNGNQZNdOQXdy/TQUGD1r8K
      gm
75    YgP6e8J3YHRcEllmug1CV18Y08gZfBWWQ4MqkSwosBUaOduypHL48FzcDA
      3u
76    DlLNc47A+ObuCegX5GXscq7YFSQ/cjYHDgld5IRZnw99P6Pk20qoBO7blK
      VQ
77    VbnXAjXpR+S239QO1Y9L5MxLIMbJ+Wd5Jy8W7iXQ8PdKDnlvUunXBches1
      gG
78    71bTyFPBbhG0PB6Sm0xtObwq6iYD2TI1FP4oSbG0ehA2zWhIuX5rES73G1
      Zh
79    guNMYr3mOkqcKVDkGJfCUOY86eV7vj443VHab7ieaf+Fl8P8sE9Op/hgbp
      9l
80    FcrP2EX4D2xpFVo=
81    "]]
```

```
82    }, Open  ]],

83    Cell[CellGroupData[{

84    Cell["K1 (mol/Kgcat.s)", "Subsection",
85    CellChangeTimes->{{3.7346806169801683`*^9,
      3.7346806764644165`*^9}, {
86    3.7474953314044094`*^9, 3.747495334513953*^9}}],

87    Cell[BoxData[{
88    RowBox[{
89    RowBox[{"k1klose", "=",
90    RowBox[{"k0klose", "*",
91    SuperscriptBox["\[ExponentialE]",
92    FractionBox[
93    RowBox[{"-", "E1"}],
94    RowBox[{"R", "*", "Tg"}]]]]}]}], ";"}],
      "\[IndentingNewLine]",
95    RowBox[{
96    RowBox[{"k1zhang", "=",
97    RowBox[{"k0zhang", "*",
98    SuperscriptBox["\[ExponentialE]",
99    FractionBox[
100   RowBox[{"-", "E1"}],
101   RowBox[{"R", "*", "Tg"}]]]]}]}], ";"}]}], "Input",
102   CellChangeTimes->{{3.7346806810281754`*^9,
      3.7346807731013703`*^9}, {
103   3.7346808093550644`*^9, 3.7346808425049963`*^9},
      {3.734680887599244*^9,
104   3.734680926246883*^9}, {3.7346820555866137`*^9,
      3.7346820861209354`*^9}, {
105   3.747462373959881*^9, 3.7474623766628685`*^9},
      {3.74749534325321*^9,
106   3.7474953474506373`*^9}}]
107   }, Open  ]],

108   Cell[CellGroupData[{

109   Cell["Adsorption constants", "Subsection",
110   CellChangeTimes->{{3.734681232702321*^9,
      3.7346812388000984`*^9}, {
111   3.7474953925139637`*^9, 3.7474954056813707`*^9}}],

112   Cell[BoxData[{
113   RowBox[{
114   RowBox[{"Kc", "=",
115   RowBox[{"K0c", "*",
116   SuperscriptBox["\[ExponentialE]",
117   FractionBox[
118   RowBox[{"-", "\[CapitalDelta]Hc"}],
119   RowBox[{"R", "*", "Tg"}]]]]}]}], ";"}],
      "\[IndentingNewLine]",
120   RowBox[{
121   RowBox[{"Kh", "=",
122   RowBox[{"K0h", "*",
123   SuperscriptBox["\[ExponentialE]",
124   FractionBox[
125   RowBox[{"-", "\[CapitalDelta]Hh"}],
```

```
126   RowBox[{"R", "*", "Tg"}]]]}]}], ";"}]}], "Input",
127   CellChangeTimes->{{3.7346812457475576`*^9,
      3.734681252760999*^9}, {
128   3.7346813254569407`*^9, 3.734681469231891*^9},
      {3.7474623788745537`*^9,
129   3.7474623813553104`*^9}}]
130   }, Open  ]]
131   }, Open  ]],

132   Cell[CellGroupData[{

133   Cell["Rate (mol CO converted / Kgcat . s)", "Section",
134   CellChangeTimes->{{3.7335537793597965`*^9,
      3.733553780399412*^9}, {
135   3.7347574332064962`*^9, 3.734757485957302*^9},
      {3.7347776503211823`*^9,
136   3.734777657040663*^9}, {3.734777693138362*^9,
      3.7347777137342834`*^9}, {
137   3.747495421029964*^9, 3.7474954460768843`*^9}}],

138   Cell[CellGroupData[{

139   Cell["Co", "Subsection",
140   CellChangeTimes->{{3.7337465773153987`*^9,
      3.7337465951951585`*^9}, {
141   3.7347563336982384`*^9, 3.73475633800844*^9},
      {3.7474953699815083`*^9,
142   3.747495370715741*^9}}],

143   Cell[BoxData[
144   RowBox[{
145   RowBox[{"rb", "=",
146   RowBox[{"A", "*",
147   FractionBox[
148   RowBox[{
149   SuperscriptBox["Ph2", "0.75"], "*", "Pco"}],
150   SuperscriptBox[
151   RowBox[{"(",
152   RowBox[{"1", "+",
153   RowBox[{"K1co", "*", "Pco"}]}], ")"}], "2"]], "*",
154   RowBox[{"10", "^",
155   RowBox[{"-", "3"}]}]}]}]}], ";"}]], "Input",
156   CellChangeTimes->{{3.733553783389987*^9,
      3.7335539363289504`*^9},
157   3.7335547522128396`*^9, 3.7337466639837494`*^9,
      {3.7347563017647295`*^9,
158   3.734756321243659*^9}, {3.734757119101571*^9,
      3.7347571220789337`*^9},
159   3.747462390656242*^9}]
160   }, Open  ]],

161   Cell[CellGroupData[{

162   Cell["Fe", "Subsection",
163   CellChangeTimes->{{3.7347556708534064`*^9,
      3.7347556798857565`*^9}, {
164   3.734756341812559*^9, 3.734756343338107*^9},
      {3.747495373294588*^9,
```

```
3.7474953739975615`*^9}}],

Cell[BoxData[
RowBox[{
RowBox[{"rf", "=",
RowBox[{"A", "*",
FractionBox[
RowBox[{
SuperscriptBox["Ph2", "0.75"], "*", "Pco"}],
SuperscriptBox[
RowBox[{"(",
RowBox[{"1", "+",
RowBox[{"K2co", "*", "Pco"}]}], ")"}], "2"]], "*",
RowBox[{"10", "^",
RowBox[{"-", "3"}]}]}]}]}], ";"}]], "Input",
CellChangeTimes->{{3.734755687473586*^9,
3.7347557726223297`*^9},
3.7347558198991933`*^9, 3.7347562861188893`*^9,
{3.734756362683694*^9,
3.7347563636534224`*^9}, {3.7347571246617136`*^9,
3.734757131250533*^9},
3.7347773350676713`*^9, 3.734777429422961*^9,
3.7474623954440546`*^9}]
}, Open  ]],

Cell[CellGroupData[{

Cell["18%Ni", "Subsection",
CellChangeTimes->{{3.7337466307803264`*^9,
3.7337466540543585`*^9}, {
3.747495377482283*^9, 3.7474953801693783`*^9}}],

Cell[BoxData[
RowBox[{
RowBox[{"r18", "=",
FractionBox[
RowBox[{"k1klose", "*", "Kc", "*",
SuperscriptBox["Kh", "2"], "*",
SuperscriptBox["Pco", "0.5"], "*", "Ph2"}],
SuperscriptBox[
RowBox[{"(",
RowBox[{"1", "+",
RowBox[{"Kc", "*",
SuperscriptBox["Pco", "0.5"]}], "+",
RowBox[{"Kh", "*",
SuperscriptBox["Ph2", "0.5"]}]}], ")"}], "3"]]}], ";"}]],
"Input",
CellChangeTimes->{
3.7337466674966874`*^9, {3.734680968205062*^9,
3.734681125757468*^9},
3.7474623988121824`*^9}]
}, Open  ]],

Cell[CellGroupData[{

Cell["50%Ni", "Subsection",
CellChangeTimes->{{3.734681149920385*^9,
3.7346811525167065`*^9}, {
```

```
3.7474953837477026`*^9, 3.747495386576936*^9}}],

Cell[BoxData[
RowBox[{
RowBox[{"r50", "=",
FractionBox[
RowBox[{"k1zhang", "*", "Kc", "*",
SuperscriptBox["Kh", "2"], "*",
SuperscriptBox["Pco", "0.5"], "*", "Ph2"}],
SuperscriptBox[
RowBox[{"(",
RowBox[{"1", "+",
RowBox[{"Kc", "*",
SuperscriptBox["Pco", "0.5"]}], "+",
RowBox[{"Kh", "*",
SuperscriptBox["Ph2", "0.5"]}]}]}], ")"}], "3"]}]}], ";"}]],
"Input",
CellChangeTimes->{{3.734681164062151*^9,
3.7346811674575386`*^9}, {
3.734681931759965*^9, 3.734681951796131*^9},
{3.73486904205091*^9,
3.734869042293314*^9}, 3.7474624023537607`*^9}]
}, Open  ]]
}, Open  ]]
}, Open  ]]
},
WindowSize->{1118, 966},
WindowMargins->{{-8, Automatic}, {Automatic, 0}},
SpellingDictionaries->{"CorrectWords"->{"Adsorption"}},
Magnification:>1.5 Inherited,
FrontEndVersion->"11.0 for Microsoft Windows (64-bit)
(September 21, 2016)",
StyleDefinitions->FrontEnd`FileName[{"Report"},
"StandardReport.nb",
CharacterEncoding -> "UTF-8"]
]
(* End of Notebook Content *)

(* Internal cache information *)
(*CellTagsOutline
CellTagsIndex->{}
*)
(*CellTagsIndex
CellTagsIndex->{}
*)
(*NotebookFileOutline
Notebook[{
Cell[CellGroupData[{
Cell[580, 22, 110, 1, 147, "Title"],
Cell[CellGroupData[{
Cell[715, 27, 198, 3, 109, "Section"],
Cell[CellGroupData[{
Cell[938, 34, 125, 2, 54, "Subsection"],
Cell[1066, 38, 2016, 56, 462, "Input"]
}, Open  ]],
Cell[CellGroupData[{
Cell[3119, 99, 159, 2, 54, "Subsection"],
Cell[3281, 103, 762, 19, 119, "Input"]
```

```
260   }, Open  ]],
261   Cell[CellGroupData[{
262   Cell[4080, 127, 163, 2, 54, "Subsection"],
263   Cell[4246, 131, 623, 17, 121, "Input"]
264   }, Open  ]]
265   }, Open  ]],
266   Cell[CellGroupData[{
267   Cell[4918, 154, 323, 4, 109, "Section"],
268   Cell[CellGroupData[{
269   Cell[5266, 162, 195, 3, 54, "Subsection"],
270   Cell[5464, 167, 595, 16, 94, "Input"]
271   }, Open  ]],
272   Cell[CellGroupData[{
273   Cell[6096, 188, 194, 3, 54, "Subsection"],
274   Cell[6293, 193, 643, 16, 94, "Input"]
275   }, Open  ]],
276   Cell[CellGroupData[{
277   Cell[6973, 214, 148, 2, 54, "Subsection"],
278   Cell[7124, 218, 550, 16, 100, "Input"]
279   }, Open  ]],
280   Cell[CellGroupData[{
281   Cell[7711, 239, 146, 2, 54, "Subsection"],
282   Cell[7860, 243, 620, 16, 100, "Input"]
283   }, Open  ]]
284   }, Open  ]]
285   }, Open  ]]
286   }
287   ]
288   *)
```